Temporal Dynamics and Stoichiometry in Notch Signaling - from Notch Synaptic Complex Formation to NICD Nuclear Entry

Lena Tveriakhina[1,9], Gustavo Scanavachi[2,3,9], Emily D. Egan[1], Ricardo Bango Da Cunha Correia[2,3], Alexandre P. Martin[1], Julia M. Rogers[1], Jeremy S. Yodh[5], Jon C. Aster[6], Tom Kirchhausen[2,3,4*], Stephen C. Blacklow[1,7,8,9,*]

[1]Department of Biological Chemistry and Molecular Pharmacology, Blavatnik Institute, Harvard Medical School, Boston, MA 02115, USA.

[2]Department of Cell Biology, Harvard Medical School, Boston, MA 02115, USA.

[3]Program in Cellular and Molecular Medicine, Boston Children's Hospital, Boston, MA 02115, USA;

[4]Department of Pediatrics, Harvard Medical School, Boston, MA 02115, USA.

[5]Department of Physics, Harvard University, Cambridge, MA 02138, USA.

[6]Department of Pathology, Brigham and Women's Hospital, Boston, MA 02115, USA.

[7]Department of Cancer Biology, Dana Farber Cancer Institute, Boston, MA 02215, USA.

[8]Lead contact

[9]These authors contributed equally.

[*]Correspondence: kirchhausen@crystal.harvard.edu (T.K.), stephen_blacklow@hms.harvard.edu (S.C.B.)

Abstract/Summary (150 words)

Mammalian Notch signaling occurs when binding of Delta or Jagged to Notch stimulates proteolytic release of the Notch intracellular domain (NICD), which enters the nucleus to regulate target gene expression. To determine the temporal dynamics of events associated with Notch signaling under native conditions, we fluorescently tagged Notch and Delta at their endogenous genomic loci and visualized them upon pairing of receiver (Notch) and sender (Delta) cells as a function of time after cell contact. At contact sites, Notch and Delta immediately accumulated at 1:1 stoichiometry in synapses, which resolved by 15-20 min after contact. Synapse formation preceded entrance of the Notch extracellular domain into the sender cell and accumulation of NICD in the nucleus of the receiver cell, which approached a maximum after ~45 min and was prevented by chemical and genetic inhibitors of signaling. These findings directly link Notch-Delta synapse dynamics to NICD production with unprecedented spatiotemporal precision.

Keywords

Notch, Delta, synapses, signal transduction, transendocytosis, receptor, transcription, NICD, LLSM

Introduction

Notch signaling influences critical cell fate decisions in all metazoans and regulates tissue homeostasis in adults (Bray, 2016; Kovall et al., 2017; Sprinzak & Blacklow, 2021). The essential role of Notch signaling during development is evident from the embryonic lethality associated with deficiencies in Notch signaling in various model organisms, including worms, flies, and mice (Bray, 2016).

Aberrant Notch signaling is also associated with a variety of human pathologies. Germ-line mutations of core components of Notch signaling result in disorders such as Alagille syndrome, caused by loss of function mutations in *NOTCH2* or *JAGGED1* (Kamath et al., 2012; Li et al., 1997; Oda et al., 1997), and the stroke syndrome CADASIL, caused by missense mutations in the gene encoding *NOTCH3* (Joutel et al., 1996). Oncogenic gain-of-function mutations in human *NOTCH1* are frequently found in human T cell acute lymphoblastic leukemia/lymphoma (T-ALL) (Weng et al., 2004), certain B cell malignancies (Puente et al., 2011), and some solid tumors (Aster et al., 2017). Genomic studies have also uncovered loss-of-function mutations of *NOTCH1*, *NOTCH2*, and *NOTCH3* in squamous cell carcinomas in the skin, head and neck (Agrawal et al., 2011; Wang et al., 2011), and in precancerous regions of sun-exposed skin (Martincorena et al., 2015).

Mammals have four Notch receptors (NOTCH1-4) and four well-characterized activating ligands (DLL1, DLL4, JAG1, and JAG2). The Notch proteins are single-pass transmembrane receptors that are normally processed during maturation by a furin-like protease at an extracellular site called S1 (Blaumueller et al., 1997; Logeat et al., 1998)

44 to generate non-covalently associated extracellular (NECD) and transmembrane (NTM)
45 subunits. The mature heterodimeric receptor normally resides on the cell surface of the
46 signal-receiving cell (or receiving cell) in an autoinhibited or “off” state and signaling is
47 initiated at sites of cell-cell contact when Notch proteins on a receiver cell bind to Delta
48 or Jagged ligands on a sender cell. Ligand binding relieves Notch autoinhibition by
49 inducing proteolysis by the ADAM10 metalloprotease at a membrane proximal site called
50 S2, producing a truncated transmembrane subunit called NEXT (for Notch extracellular
51 truncation). NEXT becomes a substrate for the intramembrane protease gamma-
52 secretase (γ-secretase), which cleaves Notch near the inner membrane leaflet at site S3.
53 This proteolytic step releases the Notch intracellular domain (NICD), which translocates
54 into the nucleus and forms a multiprotein complex with the DNA-binding transcription
55 factor RBPJ, a protein of the Mastermind-like family (MAML) and additional co-activators
56 to induce Notch target gene transcription (Bray, 2016; Sprinzak & Blacklow, 2021). The
57 fate of the Notch extracellular domain (NECD) is less clear, but studies suggest a model
58 in which it is endocytosed into the sender cell in complex with ligand, a process that
59 depends on the E3 ubiquitin ligase Mindbomb (MIB) (Daskalaki et al., 2011; Guo et al.,
60 2016; McMillan et al., 2015; Okano et al., 2016).
61
62 Although these steps of Notch signaling have been studied since *Drosophila*
63 *melanogaster* Notch was cloned 40 years ago (Artavanis-Tsakonas et al., 1983), how
64 these events are temporally coupled and choreographed during signaling is less well
65 understood. Likewise, it is not known what the receptor-ligand stoichiometry is when
66 complexes form at the membrane, nor is it clear how efficiently ligand-receptor
67 engagement at the membrane leads to NICD production. Moreover, time-resolved linkage

68 of the ligand-receptor interaction to internalization of NECD into sender cells has not been
69 directly observed.
70
71 Using fluorescence microscopy in fly or mammalian cells transiently or stably
72 overexpressing ligand and/or receptor molecules, others have shown that at sites of direct
73 cell-cell contact, Notch and its ligands can gather and form stable clusters (Chapman et
74 al., 2016; Fehon et al., 1990; Klueg & Muskavitch, 1999; Meloty-Kapella et al., 2012;
75 Nichols et al., 2007). Similarly, transendocytosis of the NECD into vesicular structures
76 within sending cells has also been observed in cell culture and in flies (Nichols et al.,
77 2007; Parks et al., 2000). Ectopic overexpression of Notch can also result, however, in
78 intracellular retention, mislocalization, and clustering of receptor molecules within the ER
79 (Chapman et al., 2011; Mumm et al., 2000; van Tetering et al., 2009), raising the
80 possibility that these findings are not physiologically representative. It is therefore
81 important to use tagged Notch proteins expressed from endogenous loci to ensure faithful
82 recapitulation of the temporal dynamics of early events responsible for Notch signaling.
83
84 In the quantitative studies reported here, we combined use of volumetric spinning disk
85 confocal and lattice light-sheet microscopy (LLSM) (Chen et al., 2014) to image cells
86 expressing physiological amounts of fluorescently tagged Notch and ligand proteins
87 expressed from their endogenous loci to analyze protein localization, organization, and
88 dynamics in living cells. LLSM was chosen because it minimizes photobleaching,
89 increases signal to noise ratio, and allows for high spatiotemporal precision of time series
90 recorded from the whole cell volume. When sender and receiver cells made contact,
91 ligands and receptors clustered into synapses at the site of contact, with a synapse
92 lifetime of roughly 15-20 min and a ligand:receptor stoichiometry of 1:1. Synapse

93 formation preceded transendocytosis of NECD (and some full-length Notch) into the
94 sending cell and eventual accumulation of up to 1000-2000 NICD molecules in the
95 nucleus of the receiving cell. This work defines for the first time the stoichiometry,
96 integrated temporal order and timing of central steps in Notch signal transduction from
97 synapse formation through nuclear NICD accumulation and charts a course for studying
98 real-time Notch dependent signaling dynamics in living cells in both physiological and
99 pathophysiological contexts.

100 **Results**

101

102 **Establishment of a system to visualize Notch signaling in real time**

103

104 To study the events of physiologic Notch signaling using fluorescence microscopy in living
105 cells, we screened for Notch- and ligand-expressing cell lines that i) were amenable to
106 CRISPR/Cas9 engineering, ii) expressed one receptor or ligand endogenously at
107 substantially greater natural abundance than others, and iii) were active as either receiver
108 (Notch-expressing cells) or sender (ligand-expressing cells) cells, as assessed by assays
109 for induction of Notch-dependent gene expression.

110

111 SVG-A immortalized fetal astrocytes met these criteria as a Notch-expressing (receiver)
112 cell line. They have been previously successfully engineered using CRISPR/Cas9 (Chou
113 et al., 2016), they express vastly more *NOTCH2* than other Notch isoforms (as judged by
114 analysis of mRNA abundance by quantitative reverse-transcriptase PCR (Martin et al.,
115 2023)), and when co-cultured with U2OS cells ectopically expressing the DLL4 ligand,
116 they exhibit strong induction of a Notch-responsive luciferase reporter gene (Figure S1A,
117 related to Figure 1). The reporter response was blocked by treatment with a γ-secretase
118 inhibitor (GSI; Compound E) (Figure S1A, related to Figure 1) and was not observed in
119 co-culture assays with parental U2OS cells. The transcriptional response to co-culture
120 with ligand-expressing cells was also greatly reduced when *NOTCH2* was knocked out
121 of SVG-A cells using CRISPR/Cas9 (Figure S1A, related to Figure 1), confirming that
122 NOTCH2 was responsible for most Notch signaling activity in these cells. Importantly,
123 when SVG-A cells were plated in tissue culture dishes containing immobilized JAG1,
124 sentinel Notch target genes were induced within 2 to 4 hours (*e.g. HES1, TRIB1*), and the

125 “Notch Signaling Pathway” Gene Ontology term (Chen et al., 2013; Kuleshov et al., 2016)
126 was enriched among genes induced at 2, 4, and 24 hours after stimulation (Figure S1B,
127 related to Figure 1).
128
129 We identified two ligand-expressing (signal-sending) cell lines that met our criteria. The
130 first sender cell line was DMS53, which expresses DLL4 as its predominant ligand and is
131 able to activate Notch as judged by the induction of reporter gene expression in SVG-A
132 receiver cells (Figure S2, related to Figure 1). Knockout of DLL4 in DMS53 cells also
133 reduced signal-sending activity (Figure S2H, related to Figure 1), with residual ligand
134 activity likely resulting from the expression of other ligands (Figure S2A,B, related to
135 Figure 1). The second sender line was A673, which endogenously expresses JAG1 as
136 its predominant ligand (Figure S3, related to Figure 1) and induces a Notch reporter
137 response in SVG-A receiver cells (Figure S3C, related to Figure 1). Knockout of JAG1 in
138 A673 cells abrogated their signal sending activity (Figure S3H, related to Figure 1),
139 consistent with the observation that JAG1 was the only ligand detectable in these cells
140 by flow cytometry (Figure S3A,B, related to Figure 1).
141
142 We used CRISPR/Cas9 in SVG-A, DMS53, and A673 cells to fuse fluorescent proteins
143 or HaloTags (Los et al., 2008) to Notch and ligand proteins in their endogenous loci for
144 expression at natural abundance. In SVG-A cells, NOTCH2 was double-tagged with
145 mNeonGreen (mNeon) (Shaner et al., 2013) inserted after the signal peptide to position
146 it extracellularly at the mature N-terminus of the NECD subunit, and with a HaloTag
147 inserted after A2471 to place a second fluorophore intracellularly at the C-terminus of the
148 NTM subunit (Figure 1A, Figure S4, related to Figure 1). These labeling positions are
149 hereafter specified as N2-N and N2-C, respectively. In DMS53 and A673 cells, a HaloTag

150 was fused to the C-terminal end of DLL4 or JAG1, respectively (Figure 1A,B, Figure S2D-
151 F, Figure S3D-F, related to Figure 1). The steady-state expression amount and signaling
152 activity of tagged receptor and ligand proteins were not substantially altered when
153 compared to the endogenous proteins in parental cells, confirming that the tags do not
154 disrupt protein processing or function (Figure S2G-J, Figure S3G-J, Figure S4E-H, related
155 to Figure 1).
156
157 We engineered a microfluidics device for imaging in a confocal (SD) or lattice light-sheet
158 microscope (LLSM). The device made it possible to pair cells and observe the cell pairs
159 in real time from the moment of initial contact, allowing us to follow the dynamics of
160 NOTCH2 and DLL4 associated with signal transmission (Figure 1C, Figure S5, related to
161 Figure 1). Sender and receiver cells were separately labeled with HaloTag ligands
162 conjugated to different JaneliaFluorX (JFX) dyes (Grimm et al., 2020) prior to pairing. The
163 sender cells were then delivered to receiver cells pre-plated on the cover slip by passage
164 through a microfluidic chip using a pressure-controlled pump.
165
166 **Notch synapses form between NOTCH2 and DLL4 at sites of cell-cell contact**
167
168 In cultured SVG-A cells, NOTCH2 was found at the plasma membrane and in intracellular
169 puncta (Figure 1D, Figure S6A, related to Figure 1) that likely represent trafficking
170 vesicles and/or organelles related to protein synthesis and degradation. The concurrent
171 presence of nonspecific or autofluorescence signals in the green (488) and red (561)
172 channels, also seen as small intracellular puncta in both parental cells and in knockin
173 cells that did not have a JFX dye coupled to the HaloTag (Figure S6A,B, related to Figure

174 1), prevented unambiguous identification of NOTCH2-containing vesicles inside these
175 cells.
176
177 DMS53 sender cells delivered to the SVG-A receiver cells allowed real time imaging of
178 DLL4 engagement with NOTCH2 at sites of contact (Figure 1C,D). These sites, which we
179 defined as Notch synapses, showed accumulation of NOTCH2 and DLL4 and presumably
180 occurred at sites of molecular contact between the ectodomains of DLL4 and NOTCH2
181 (Figure 1D, Movies 1, 2A,B). Synapses formed with 100% efficiency within seconds every
182 time these two cell types made direct contact and varied in size and shape (Figure S7A,
183 related to Figure 1). Preincubation of DMS53 cells with ligand-blocking antibodies
184 prevented synapse formation and effectively silenced signaling (Figure S7B,C, related to
185 Figure 1), indicating that synapse formation required direct binding of DLL4 to NOTCH2.
186
187 To evaluate whether the proteins concentrated at points of cell-cell contact, we compared
188 the fluorescence intensities of the N2-N, N2-C, and DLL4 tags in synapses to their
189 intensities in membrane regions excluded from the synapses ("membrane") and
190 measured significantly higher fluorescence intensity signals in the synapses (Figure 1E).
191
192 We determined the ratio of fluorescence intensities of the N2-N and N2-C tags in the
193 membrane of receiving cells (before delivery of ligand cells), and set the value of that ratio
194 to a stoichiometry of 1:1 because both fluorophores are coupled to the same receptor
195 protein. The same 1:1 stoichiometry was observed outside synapses after Notch cells
196 contacted sender cells (Figure 1F; N2-N/N2-C in membrane). The N2-N:N2-C
197 stoichiometry remained 1:1 in synapses associated with NOTCH2 - DLL4 engagement
198 (Figure 1F; N2-N/N2-C in synapse). To determine the stoichiometric ratio of NOTCH2 to

199 DLL4 in synapses, we exploited the capacity of the HaloTag to be labeled with different
200 dyes and exchanged the Notch C-terminal and DLL4 fluorophores to determine the
201 NOTCH2:DLL4 ratio in the synapse. We established that the N2-N to N2-C and N2-N to
202 DLL4 fluorescent tag ratios were 1:1 independent of the dyes exchanged and
203 indistinguishable from each other (Figure 1F; N2-N/N2-C and N2-N/DLL4 in synapse).
204
205 Similarly, a 1:1 receptor:ligand stoichiometry was present at synapses formed by
206 NOTCH2 and JAG1 upon pairing A673 JAG1-HaloTag cells and NOTCH2-tagged SVG-
207 A cells (Figure S3L,M, related to Figure 1). One detectable difference was that the A673
208 (JAG1) cells formed synapses less efficiently than the DMS53 (DLL4) cells (Figure S3N,
209 related to Figure 1), most likely because the amount of JAG1 on the surface of A673 cells
210 was lower than the amount of DLL4 on DMS53 cells. In each case, endogenously
211 expressed ligands and receptors formed synapses at contact sites in living cells with a
212 stoichiometry of 1:1.
213
214 **NOTCH2 and DLL4 in synapses do not readily exchange**
215
216 We performed fluorescence recovery after photobleaching (FRAP) in a spinning disk
217 confocal microscope to assess the dynamics of receptor and ligand exchange on the cell
218 surface, both in regions outside of and within synapses. FRAP was performed within a
219 region of interest (ROI) and recovery was monitored at 1 s intervals for a total of 60 s.
220 Outside sites of cell contact, the fluorescence intensity after bleaching recovered 80%-
221 90% of the initial value after 60 s for both the N2-N and N2-C tags and for the DLL4 tag,
222 indicating that both proteins are mobile on the cell surface (Figure 2A,B). The half-times
223 for recovery ($t_{1/2}$) of N2-N and N2-C on SVG-A cells were 7.5±2.5 and 7.2±3.0 s, which

224 correspond to diffusion coefficients (D) of 0.053±0.02 $\mu m^2 s^{-1}$ and 0.057±0.02 $\mu m^2 s^{-1}$,
225 respectively (Figure 2B,C). Free DLL4 molecules on the surface of DMS53 cells had a
226 similar mobility, with a recovery $t_{1/2}$ of 4.7±1.6 s and a diffusion coefficient of 0.061±0.024
227 $\mu m^2 s^{-1}$ (Figure 2B,C). These diffusion coefficients are comparable to that of stably
228 overexpressed DLL1 in CHO-K1 cells (Khait et al., 2016) and to those of other freely
229 diffusing membrane proteins (Jacobson et al., 1987).
230
231 We next determined the mobility of Notch and DLL4 molecules at the synapse by
232 bleaching the fluorophore of interest 5-10 min after the onset of synapse formation. We
233 monitored the fluorescence intensity of the non-bleached component within the region of
234 interest (ROI) to delineate the synapse's location and ascertain its structural integrity
235 throughout the 60-second observation period (Figure 2D,F,H). In contrast to the rapid
236 fluorescence recovery of N2-N, N2-C or DLL4 in the surrounding cell surface membrane,
237 NOTCH2 or DLL4 did not readily exchange when in synapses (10-20% recovery after 60
238 s) (Figure 2E,G,I). Thus, at the site of contact, both receptor and ligand exhibited greatly
239 reduced exchange within the synapse and/or with the surrounding membrane.
240
241 **Notch transendocytosis into the sender cell occurs after synapse formation**
242
243 Transendocytosis of NECD and full-length Notch into ligand cells has been observed in
244 cultured cells (Nichols et al., 2007; Parks et al., 2000) and in flies (Langridge & Struhl,
245 2017; Parks et al., 2000). Here, we monitored transendocytosis of NOTCH2, which
246 accumulated into puncta within DMS53 (DLL4) cells only after synapse formation
247 between paired cells (Figure 3A,B, Movie 3). We quantified the relative amounts and
248 stoichiometry of the N2-N (*i.e.* NECD) and N2-C tags to the DLL4 tag in these puncta by

249 determining the fluorescence intensity ratios of different fluorophore pairs in these
250 structures 60 min after synapse formation. The N2-N (*i.e.* NECD) to DLL4 stoichiometric
251 ratio was approximately 1:1 (Figure 3C; left, n = 174 puncta) in agreement with the ratio
252 of receptor to ligand in synapses. In 54 of the puncta, only the N2-N (*i.e.* NECD) and DLL4
253 were detected (Figure 3C; middle), whereas in the other puncta some N2-C was present
254 along with N2-N and DLL4 (Figure 3C; right), indicative of occasional transendocytosis of
255 full-length NOTCH2 as well as just the NECD. Quantification of the N2-N/N2-C ratio in
256 these puncta showed an average value of 4:1, with considerable variation among the
257 puncta.
258
259 While the majority of transendocytosis events involved only or predominantly N2-N (*i.e.*
260 NECD), the entry of some N2-C into ligand cells along with N2-N suggested that some
261 non-productive transendocytosis of full-length receptors occurred. Consistent with this
262 interpretation, we did not observe any evidence of Notch signaling activity when ligand
263 (DMS53) cells were probed using a luciferase reporter for a NICD-dependent response
264 (Figure S8, related to Figure 3), and we did not observe any accumulation of NICD in the
265 nuclei of those cells. We also did not detect entry of DLL4 into the SVG-A (NOTCH2)
266 receiver cells.
267
268 Occasionally, we were able to observe vesicle-like structures containing both ligand and
269 receptor adjacent to synapse sites (Figure 3D). While our analyses did not allow us to
270 determine unambiguously whether these vesicles originated directly from synapses or if
271 the NOTCH2 and DLL4 instead accumulated in vesicles residing close to the contact site,
272 it is possible these objects are vesicles captured at a very early stage shortly after
273 initiation of transendocytosis.

274

275 **Quantification of nuclear entry of NICD after cell contact**

276

277 NICD can access the nucleus within 30 min of γ-secretase inhibitor removal (Martin et al.,
278 2023) and can induce a transcriptional response in the nucleus within 60 min of Notch
279 activation (Falo-Sanjuan & Bray, 2022; Ilagan et al., 2011). To quantify the amount of N2-
280 C entering nuclei after cell-cell contact, we paired and imaged sender and receiver cells
281 immediately (1-5 min) and 60 min after cell contact. Visual inspection of the nuclear region
282 showed an increase of the fluorescent signal of N2-C, consistent with NICD nuclear entry
283 (Figure 4A). The nuclear N2-C (*i.e.* NICD) concentration, calculated using a calibration
284 curve with purified, recombinant HaloTag protein in solution labeled with JFX549 (Figure
285 S9, related to Figure 4), rose from 0.65±0.6 nM before or immediately after cell contact
286 to ~2±1.1 nM (equivalent to ~1000-2000 NICD molecules) at a time point 60 minutes after
287 synapse formation (Figure 4B,C). The presence of intracellular puncta in the isolated
288 NOTCH2 cells did not allow us to unambiguously follow the path of N2-C (*i.e.* NICD) from
289 the synapse to the nucleus.

290

291 **Temporal linkage between Notch processing and nuclear entry in living cells**

292

293 We next established a quantitative spatiotemporal link among synapse formation, NECD
294 transendocytosis, and NICD nuclear accumulation by using our microfluidic device to
295 obtain imaging data of nine cell pairing events with a lattice light-sheet microscope over
296 a 60-minute time course (Figure 5 and Figure S10, related to Figure 5). This approach
297 enabled three-dimensional (3D) visualization with little photobleaching and phototoxicity
298 compared to conventional spinning disk microscopes, thereby allowing repeated

299 quantitative imaging of fluorescently tagged proteins expressed at endogenous levels
300 over a prolonged period of time. The signal distribution of NOTCH2 at the cell surface
301 was homogeneous in the absence of contact with DMS53 sender cells (t=0), as assessed
302 by analysis of N2-N and N2-C tag fluorescence, and the nuclear N2-C signal was minimal
303 (Figure 5A,B). Again, Notch synapses rapidly formed at the site of contact between
304 sender and receiver cells; NOTCH2 and DLL4 molecules accumulated within seconds
305 after contact and the average synapse grew (assessed by the N2-N signal) from roughly
306 500 NOTCH2 molecules after 5 min of contact to a peak of roughly 2000 molecules at
307 15-20 min. After 30 min, the synapses typically resolved (Figure 5 and Figure S10, related
308 to Figure 5). The number of N2-N (*i.e.* NECD) molecules in puncta of DMS53 sender cells
309 increased to a maximum at roughly 15 minutes before slowly decaying after 40 min,
310 perhaps due to protein degradation, entry into a compartment with a different pH, or both
311 (Figure 5). Finally, the concentration of N2-C (*i.e.* NICD) in the nuclei of the receiver cells
312 increased to a maximum of 1.42±0.41 nM, corresponding to 1000-2000 molecules ~45
313 minutes after cell-cell contact, and remained steady until the end of the 60 min time course
314 (Figure 5).
315
316 **Mindbomb, ADAM10, and γ-secretase are not essential for synapse formation but**
317 **are required for nuclear entry of NICD**
318
319 The E3 ubiquitin ligase Mindbomb1 (MIB1) is required in sender cells for ligand activity
320 and subsequent receptor activation (Guo et al., 2016). We eliminated *MIB1* in DLL4-
321 HaloTag cells (*MIB1ko*) using CRISPR/Cas9 (Figure S11A,B, related to Figure 6) and
322 paired these cells with our tagged SVG-A cells to monitor synapse formation, Notch
323 transendocytosis, and N2-C accumulation in the nuclei of Notch cells. *MIB1ko* cells

324 formed synapses efficiently but these synapses did not resolve after 60 min (Figure 6A).
325 *MIB1ko* cells were also unable to induce transendocytosis of N2-N (*i.e.* NECD) (Figure
326 5B), and failed to produce a substantial increase in nuclear N2-C (*i.e.* NICD) within
327 receiver cells (Figure 6C,D). These data show that MIB1 in sender cells is essential for
328 synapse dissolution, and confirm it is required both for endocytosis of ligand-NECD
329 complexes into the sender cell and for nuclear entry of NICD in the receiver cell.
330
331 We used protease inhibitors to investigate how preventing ADAM10 or γ-secretase
332 cleavage of Notch affects the behavior of DLL4 and NOTCH2 after cell pairing. While
333 synapses still rapidly formed after contact (Figure S11C, related to Figure 6), they
334 resolved when cleavage at S2 was prevented with the metalloprotease inhibitor
335 GI254023X. This resolution may be due in part to transendocytosis of intact NOTCH2 into
336 the sender cells because the ratio of signals from the N2-N and N2-C labels was 1:1 in
337 the internalized structures (Figure 6E), indicating that ADAM10 inhibition did not interfere
338 with the transendocytosis of full-length receptors. As expected, accumulation of N2-C (*i.e.*
339 NICD) in receiver cell nuclei was greatly reduced (Figure 6F,G). Sender and receiver cell
340 pairs also formed Notch synapses that resolved within 60 min in the presence of a γ-
341 secretase inhibitor (GSI; Compound E). Under these conditions, transendocytosis of N2-
342 N (*i.e.* NECD) and full-length NOTCH2 into sender cells was not affected when compared
343 to untreated cells (Figure 6E), indicating that release of the NECD by ADAM10 proteolysis
344 was still occurring. As expected, we failed to observe any increase in the nuclear content
345 of N2-C (*i.e.* NICD) even 60 min after initiation of cell-cell contact (Figure 6F,G); these
346 observations confirmed that γ-secretase was required for the cleavage step that produces
347 NICD and for its subsequent entry into the nucleus.
348

349 **Discussion**

350

351 In this work, we directly visualized NOTCH2 and DLL4 proteins from the onset of contact
352 between DLL4 sender and NOTCH2 receiver cells until nuclear NICD in the receiver cells
353 accumulated to steady state. A critical feature of this study was the use of genome edited
354 cells to ensure that the fluorescently tagged proteins were present at their natural
355 abundance. Using quantitative fluorescence microscopy, we uncovered the appearance
356 of a transient structure at the contact site between DLL4 sender and NOTCH2 receiver
357 cells, here termed a Notch synapse. The Notch in the synapse is the source of the NICD
358 that accumulates in the nucleus of the receiver cell.

359

360 Notch synapses form immediately after signal sending and signal receiving cells meet, as
361 previously observed at contact sites in other model systems that used ectopic protein
362 overexpression (Chapman et al., 2016; Fehon et al., 1990; Khamaisi et al., 2022; Meloty-
363 Kapella et al., 2012; Nichols et al., 2007). In contrast to our work, which uncovered the
364 transient presence of a Notch synapse elicited immediately after sender-receiver cell
365 contact, the previous studies using overexpressed proteins instead observed stable
366 synapses that could last 24 hours or longer after their formation (Chapman et al., 2016;
367 Fehon et al., 1990; Khamaisi et al., 2022).

368

369 Strikingly, NOTCH2-DLL4 synapses accumulated normally but failed to resolve in
370 synapses created between Notch receiver and sender cells lacking the E3 ligase MIB1.
371 Because NECD (represented by the N2-N tag) from SVG-A sender cells failed to
372 transendocytose into DMS53 (DLL4) *MIB1ko* cells, we disfavor a previous model for
373 activation in which the furin-processed extracellular and transmembrane subunits of

374 Notch are mechanically induced to dissociate at site S1 prior to metalloprotease cleavage
375 (Chastagner et al., 2017; Nichols et al., 2007). Additionally, a model in which mechanical
376 force supplied by bound ligand induces subunit dissociation at site S1 also predicts that
377 ADAM10 inhibition would still be permissive of transendocytosis of liberated NECD into
378 the sender cells, yet we observed that - although treatment with an ADAM10 inhibitor
379 allowed transendocytosis of full-length NOTCH2 into the sender cells - it failed to permit
380 transendocytosis of the free NECD. Our data are instead consistent with models positing
381 that MIB1-dependent endocytosis of ligand is needed to induce ADAM10 cleavage of
382 Notch at S2 in receiver cells, thereby liberating NECD. Our results are also consistent
383 with findings in flies, in which replacement of the Notch negative regulatory region (NRR),
384 which contains the S1 and S2 cut sites, by a domain more resistant to force-induced
385 unfolding also leads to transendocytosis of full-length receptors, but not free NECD, into
386 sender cells (Langridge & Struhl, 2017). Unlike the studies in flies, however, in which
387 ligands could enter the cells expressing the unfolding-resistant chimeric receptors, we did
388 not observe entry of any DLL4 into the SVG-A receiver NOTCH2 cells when ADAM10
389 cleavage was chemically inhibited.
390
391 We showed that both NOTCH2 and DLL4 were mobile when on the cell surface but
392 became fixed at the contact site once synapses formed. The mobility of DLL4 and
393 NOTCH2 outside sites of contact resembled that predicted for their lateral diffusion in the
394 membrane, and was similar to that of overexpressed DLL1 in the membranes of CHO
395 cells (Khait et al., 2016). The relative immobility of the molecules in synapses suggests
396 the existence of avidity effects that hold the molecules in place at the observed 1:1
397 stoichiometry (Figure 1).
398

399 Whether the stabilization of molecules in the synapses is a consequence of structured
400 polymerization or another mechanism of self-association among the NOTCH2 and DLL4
401 molecules is not clear. There is evidence for weak self-association of the ankyrin domains
402 of *Drosophila* Notch (Allgood & Barrick, 2011) and human NOTCH1, which contribute to
403 the cooperative formation of dimeric transcription complexes on paired site DNA (Arnett
404 et al., 2010). It is also true that the negative regulatory regions (NRRs) from NOTCH1,
405 NOTCH2, and NOTCH3 share a crystal packing interface, the disruption of which induces
406 signaling independent of ligand-receptor interaction (Gordon et al., 2009, 2007; Xu et al.,
407 2015). However, the surface density of NOTCH2 and DLL4 in synapses appears to have
408 been too low for them to be the only proteins present in synaptic sites, suggesting that
409 additional proteins are needed to form the scaffold that holds them in a synapse.
410
411 NICD accumulation could be observed in the nucleus of receiver cells as early as 10 min
412 after contact and plateaued after roughly 45 min. Live imaging of GFP-tagged Notch in
413 sensory organ precursor cells of flies has shown that Notch can be seen in the nucleus
414 on the pIIa cell as early as 10 min after cell division of the pIIa/pIIb precursor (Couturier
415 et al., 2012). The accumulation of steady-state levels of NICD in the nucleus by ~45 min
416 is also in agreement with the observed timing for transcriptional induction of Notch target
417 genes in *Drosophila* and cell culture systems (Falo-Sanjuan et al., 2019; Ilagan et al.,
418 2011; Pillidge & Bray, 2019). The timing of these dynamics are also similar to that
419 obtained by following the kinetics of proximity labeling of nuclear proteins associated with
420 the Notch transcriptional response which become labeled within 30-45 min of release
421 from GSI inhibition (Martin et al., 2023).
422

423 NICD entry into the nucleus of the receiver cell only occurred after synapse formation and
424 only when NECD entry into the sender cell was also observed. The relatively uniform
425 nuclear distribution of NICD, outside of nucleoli, from which it appeared to be excluded,
426 made it possible to estimate the number and concentration of NICD molecules in the
427 nucleus. Because the distribution of NICD in the receiver cell nuclei was not punctate, it
428 appears that NICD does not accumulate in transcriptional hubs or nuclear foci, and that
429 formation of such foci are thus not required for transcriptional induction in response to
430 NICD, at least in the first hour after cell contact.
431
432 More broadly, our studies illustrate the power of real-time imaging associated with
433 signaling dynamics using proteins labeled at natural abundance. Using this approach, we
434 uncovered dynamic formation and dissolution of synapses at sites of cell contact,
435 quantified the stoichiometry of ligand-receptor complexes in synapses, and saw directly
436 that synapse formation preceded transendocytosis of NECD into the sender cell, followed
437 by entry of NICD into the nucleus of the receiver cell. Application of this strategy to other
438 signal transduction systems should facilitate deeper understanding of their dynamics and
439 molecular mechanisms with potential to make important new contributions in the analysis
440 of complex biological systems during cell differentiation *in vitro* and *in vivo* with
441 unprecedented spatiotemporal precision.
442

Acknowledgments

We thank all members of the Blacklow and Kirchhausen laboratories for helpful discussions and encouragement. We thank Matthieu Delincé for design of the PDMS chip architecture, Luke D. Lavis and Jonathan B. Grimm for the Janelia Fluor HaloTag ligands, Tegy John Vadakkan and Eric Marino for maintaining the spinning disk confocal microscope and the Center for Nanoscale Systems at Harvard University where we produced the microfluidics devices. This work was supported by NIH awards 1R35 CA220340 (to S.C.B.), R01 CA272484 (to S.C.B. and T.K.), 5R35 GM130386 (to T.K.), and K99 GM144750 (to J.M.R.). L.T was supported by a DFG Walter-Benjamin fellowship (TV-11/1). J.C.A. was supported by the Ludwig Center at Harvard.

Author contributions

L.T., G.S., T.K and S.C.B. conceived the project. S.C.B. and T.K. acquired funding. L.T., G.S., E.D.E., R.B.D.C.C. performed experiments. L.T and G.S. analyzed the data. E.D.E. and J.M.R. processed and analyzed RNA-Seq data. A.P.M. generated A673 *JAG1ko* cells, J.S.Y. helped with the fabrication of microfluidic chips, A.P.M and J.C.A. assisted with data analysis and interpretation. L.T., G.S., T.K. and S.C.B. wrote the manuscript with input from all authors. All authors provided feedback and agreed on the final manuscript.

Declaration of interests

467 S.C.B. is on the board of directors of the non-profit Institute for Protein Innovation and the
468 Revson Foundation, is on the scientific advisory board for and receives funding from
469 Erasca, Inc. for an unrelated project, is an advisor to MPM Capital, and is a consultant for
470 IFM, Scorpion Therapeutics, Odyssey Therapeutics, Droia Ventures, and Ayala
471 Pharmaceuticals for unrelated projects. T.K. is a member of the Medical Advisory Board
472 of AI Therapeutics, Inc. J.C.A. is a consultant for Ayala Pharmaceuticals, Cellestia, Inc.,
473 SpringWorks Therapeutics, and Remix Therapeutics.
474

475 **Materials and Methods**

476

477 *Cell culture.* All cell lines were cultured at 37°C and 5% CO_2 in DMEM supplemented with
478 10% heat inactivated fetal bovine serum (FBS, GeminiBio, 100-106) and 100 U/ml
479 penicillin and streptomycin (ThermoFisher Scientific, 15140163) unless otherwise
480 specified. All cell lines were periodically tested for mycoplasma by PCR. Cells were
481 detached from plates after a PBS rinse using 0.05% Trypsin/0.53 mM EDTA in HBSS
482 (Corning) for 5-10 min at 37°C unless otherwise specified.

483

484 *Genome editing.* CRISPR/Cas9 was used for genome editing to engineer doubly tagged
485 NOTCH2 in SVG-A cells. mNeonGreen flanked by GGS (gly-gly-ser) linkers was inserted
486 after the signal peptide of NECD; HaloTag was inserted at the C-terminus of NTM after a
487 GGAG (gly-gly-ala-gly) linker sequence and immediately before the stop codon.
488 CRISPR/Cas9 editing was also used to insert a HaloTag at the C-terminus of DLL4 in
489 DMS53 cells and at the C-terminus of JAG1 in A673 cells. Halo Tag was placed between
490 a GGAG linker and immediately before the stop codon in A673 cells, or between a GGAG
491 linker and a T2A sequence preceding a neomycin resistance cassette in DMS53 cells.
492 Parental cell lines were seeded onto 6-well plates and transfected the next day with a
493 mixture of repair template (8 μg) and a pX459 plasmid (4 μg) encoding the single guide
494 RNA (gRNA) and *S. pyrogenes* Cas9 using Lipofectamine™ 2000 (Invitrogen).
495 Single SVG-A or A673 cells were sorted by fluorescence (mNeonGreen or HaloTag
496 labeled with JFX646) using a Sony SH800S Cell Sorter (Sony Biotechnology) six days
497 after transfection and collected in 50:50 conditioned:complete media (SVG-A) or 50:50
498 conditioned media:FBS (A673). Single colonies of DMS53 cells were obtained by
499 selection for 30 days using DMEM supplemented with 15% FBS (Gibco, 10437028), 100

500 U/ml penicillin and streptomycin and G418 (1 mg/ml; Geneticin, Gibco). Colonies were
501 manually picked and expanded. Successful tag integration in single colonies of all cell
502 lines was detected using genome-specific primers and PCR-based genotyping. The
503 correct sequence was then confirmed by Sanger DNA sequencing of the PCR-amplified
504 region.
505
506 Knockout of *NOTCH2* in SVG-A cells was performed by gRNA targeting of the sequence
507 downstream of the signal peptide in exon 2, and knockout of *JAG1* in A673 cells was
508 carried out with two gRNAs flanking exon 1. The gRNAs were subcloned into pX458,
509 which contains an eGFP coding sequence behind a T2A cassette downstream of the
510 gRNA insert. SVG-A or A673 cells were transfected with the gRNA-containing plasmids
511 using Lipofectamine™ 2000 (Invitrogen), and cells were allowed to grow for 3-6 days.
512 Cells were then sorted for eGFP fluorescence (indicative of plasmid uptake) using a
513 SONY SH800S Cell Sorter (Sony Biotechnology). Single SVG-A or A673 green cells were
514 collected in 50:50 conditioned:complete media or 50:50 conditioned media:FBS,
515 respectively. Cells were expanded and gene editing was confirmed by genotyping and
516 Western Blot analyses. For knockout of *DLL4* or *MIB1* in DMS53 cells, two sgRNAs
517 flanking exon1 of the target gene were subcloned into pX459 plasmids containing a
518 puromycin resistance (puroR) gene. Cells were transfected with plasmids carrying the
519 sgRNAs and were incubated in DMEM supplemented with 15% FBS (Gibco, 10437028),
520 100 U/ml penicillin and streptomycin, and puromycin (10 ug/ml) for 3 days. Puromycin
521 was removed and single colonies were allowed to grow for 30 days. Subsequently,
522 colonies were manually picked, expanded, and screened for DLL4 or MIB1 loss using
523 anti-DLL4 or anti-MIB1 antibodies by Western blot and for DLL4, by flow cytometry.
524

525 *JAGGED1-Fc expression and purification.* Human JAGGED1-Fc (Martin et al., 2023) was
526 transfected into Expi293F cells (ThermoFisher, A14527) using FectroPro (Polyplus,
527 101000007). Secreted JAGGED1-Fc was recovered from the culture media on Protein A
528 agarose (Millipore, 16-125) and eluted with 100 mM glycine, pH 3.0. The eluate was
529 neutralized with 1M HEPES buffer pH 7.3, concentrated, and buffer exchanged into 20
530 mM HEPES pH 7.3, containing 150 mM NaCl and 10% glycerol.
531
532 *RNA seq sample preparation.* SVG-A cells were removed from plates by treating with 0.5
533 mM EDTA for 3 min, quenched with media, and counted. 4 x 10^5 cells per well were plated
534 in media containing 100 nM GSI (Compound E; Millipore, 565790) on non-tissue-culture
535 treated 6-well plates that were pre-treated overnight with PBS + 0.1 mg/ml Poly-D-lysine
536 (Thermo Scientific, A3890401) and 200 μg/ml human JAGGED1-Fc. After 18 h, the SVG-
537 A cells were washed three times in 4 ml of media to remove GSI, and incubated for 2, 4,
538 or 24 hours before harvesting by resuspension in 1 ml Trizol (Thermo Scientific, 15-596-
539 026). A “0 hr” reference control was collected by performing a mock washout with media
540 containing 100 nM GSI and immediately harvesting in Trizol.
541
542 *RNA seq library construction.* Samples in Trizol were thawed, and ERCC spike-in RNAs
543 (Thermo Scientific, 4456740) were added at 10 μl per million cells. RNA was isolated
544 using chloroform following the MaXtract tube protocol (Qiagen 129056). 5 μg of RNA was
545 treated with DNaseI (Thermo Scientific, 18068015) in the presence of SUPERase-In
546 (Thermo Scientific, AM2696). RNA quality was evaluated by HS RNA ScreenTape
547 (Agilent, 5067-5579) on a TapeStation; all samples had RIN score > 8. 500 ng RNA was
548 used as input for the TruSeq Stranded Total RNA sequencing kit with RiboZero rRNA

549 depletion (Illumina, 20020598). Samples were sequenced at the Harvard University
550 Bauer Core on a NovaSeq 6000 using the S1 300 cycle kit, with paired end 150 bp reads.
551
552 *RNA seq analysis.* Reads were first mapped to ERCC spike in sequences using
553 bowtie1.2.2 with the following parameters: -n2 -l 40 -X1000 --best -3 (Langmead et al.,
554 2009). Reads not mapping to the spike-in sequences were mapped to hg38 using STAR
555 version 2.7.3a with the following arguments: --outMultimapperOrder Random --
556 outSAMattrIHstart 0 --outFilterType BySJout --outFilterMismatchNmax 4 --
557 alignSJoverhangMin 8 --outSAMstrandField intronMotif --outFilterIntronMotifs
558 RemoveNoncanonicalUnannotated --alignIntronMin 20 --alignIntronMax 1000000 --
559 alignMatesGapMax 1000000 --outWigType bedGraph --outWigNorm None --
560 outFilterScoreMinOverLread 0 --outFilterMatchNminOverLread 0 (Dobin et al., 2012).
561 Reads per gene in the Gencodev33 gtf file were counted using the featureCounts function
562 of Subread1.6.2 (Liao et al., 2013). This count matrix was used as input for DESeq2 to
563 identify differentially expressed genes, calculating each time point versus the mock
564 washout condition (Love et al., 2014). As reads mapping to the ERCC spike sequences
565 were not different between conditions, the DESeq2 size factors were used to normalize
566 samples.
567
568 *Western Blotting.* Cells were rinsed with PBS, lysed in 2x Sample buffer (0.125 M Tris pH
569 6.8, 4% SDS, 20% Glycerol, 5% β-mercaptoethanol), sonicated and boiled at 95°C for 10
570 minutes. SDS-PAGE (Mini-Protean TGX, BioRad) in 0.025 M Tris, 0.2 M Glycine, 1%
571 SDS (w/v) was followed by electrophoretic transfer to Protran nitrocellulose membrane
572 (Cytiva) using the Mini Trans-blot wet-tank transfer system (BioRad) for 70 min at 250
573 mA in Transfer Buffer (0.02 M Tris, 0.223 M Glycine, 20% methanol). Membranes were

574 stained with Ponceau Red (Fluka) to confirm successful transfer and blocked in 5% non-
575 fat dry milk in TBS-Tween buffer (TBS-T; 20 mM Tris pH 7.6, 150 mM NaCl, 0.1% Tween-
576 20) at room temperature. Incubations with primary and secondary antibodies were
577 performed in TBS-T containing 5% non-fat dry milk. Signals were detected using an
578 Odyssey CLx System (Li-Cor).
579
580 *Flow Cytometry.* Cells were rinsed with PBS and detached from cultured plates using 0.5
581 mM EDTA in PBS for 5 min at 37°C and centrifuged for 4 min at 233 *g*. Cell pellets were
582 resuspended by addition of ice-cold PBS supplemented with 2% FBS and counted using
583 a TC-20 cell counter (BioRad). 2.5-5x10^5 cells were harvested, spun down (400 *g* , 3 min,
584 4°C), and dissolved in 2% FBS in PBS containing 2.5 μl antibody. Antibody incubation
585 was performed for 1 hour at 4°C in the dark. Labeled cells were then washed 3 times with
586 500 μl 2% FBS/PBS and centrifuged for 3 min at 400 *g* and 4°C. Cell pellets were
587 dissolved in 2% FBS in PBS and flow cytometry was performed using an Accuri C6 Plus
588 (BD Biosciences) or Cytoflex Flow Cytometer (Beckman Coulter).
589
590 *Luciferase Notch reporter assay.* 0.8x10^5 SVG-A receiver cells were seeded in each well
591 of a 24-well plate. The following day, cells were transfected with 49 ng of a TP1-Luciferase
592 (Kurooka et al., 1998; Minoguchi et al., 1997) and 1 ng Renilla-Luciferase (pRL-TK,
593 Promega) using Lipofectamine™ 2000 (Invitrogen) according to manufacturers
594 instructions. 24 hours after seeding, cells were either left untreated, treated with a γ-
595 secretase inhibitor (GSI; Compound E at 0.5 μM), an ADAM10 inhibitor (GI254023X at 5
596 μM) or ligand blocking antibodies (see key resource table for concentrations). At this time,
597 1x10^5 sender cells were added to each well after they were detached from a TC dish
598 using 0.05% Trypsin/0.53 mM EDTA (Corning), and counted using a TC-20 cell counter

599 (BioRad). Approximately 24 hours after co-culture, cells were rinsed with PBS, and lysed
600 with 133 μl 1xPLB (Passive Lysis Buffer; Dual-Luciferase Reporter Assay System,
601 Promega). 10 μl of each sample was analyzed using a GloMax Discover Microplate
602 Reader (Promega) with 50 μl LARII (Luciferase Assay Reagent; Promega) and 25 μl
603 Stop&Glo solution supplemented with the Stop&Glo substate (Promega).
604
605 *Calibration of HaloTag^{JFX549} in solution.* The concentration of N2-C (*i.e.* NICD) in the
606 nucleus of SVG-A (NOTCH2) cells was estimated by using a calibration method based
607 on 3D imaging of recombinant HaloTag protein (rHaloTag) coupled to JFX549 in solution
608 using spinning disk confocal microscopy. rHaloTag was expressed in *E. coli*, purified as
609 described (Wilhelm et al., 2021) and labeled with JFX549 (the fluorophore used for
610 visualization of N2-C). Specifically, 2 μM of rHaloTag was labeled with 8 μM JFX549 (50
611 u, ~ 4x molar excess) in buffer solution (50 mM HEPES pH 7.3, 150 mM NaCl) for 25 min
612 at room temperature in a total volume of 100 μl. A Zeba™ Spin Desalting Column (7K
613 MWCO; Thermo Scientific), pre-washed three times with 100 µl of buffer solution by
614 centrifugation for 1 min at 1500 *g*, was used to remove unbound JFX549 ligand. Then,
615 rHaloTag-JFX549 was applied to the column and centrifuged for 1 min at 1500 *g*. The
616 flow-through was collected, the amount of rHaloTag determined by absorbance at 280
617 nm while the amount of JFX549 was determined by absorbance at 549 nm using a
618 NanoDrop spectrophotometer (Thermo Scientific). A fluorescence calibration curve was
619 then established by correlating the fluorescence intensity (F.I.) of solutions with different
620 concentrations of rHaloTag^{JFX549} in imaging media using the spinning disk confocal
621 microscope. Specifically, Z-stacks of 30 planes with 0.7 μm spacing between each optical
622 plane and exposure time of 100 ms (561 nm laser) were acquired. Fluorescence intensity
623 values from all planes were averaged and the background values obtained from imaging

624 of the imaging media alone was subtracted. Calibration curves were obtained by fitting a
625 linear equation to the experimental data acquired with the CCD (QuantEM, 512SC,
626 Photometrics) or sCMOS (Prism 95B, Teledyne Photometrics) cameras (Figure S9A,B).
627
628 *HaloTag and DNA labeling.* Cells were rinsed in imaging medium (Fluorobrite DMEM;
629 Gibco) supplemented with 5% FBS (GeminiBio), 25 mM HEPES pH 7.4 (Gibco), 2 mM
630 GlutaMax (Gibco), and 100 U/ml penicillin and streptomycin (Gibco). Cells were
631 subsequently incubated at 37°C for 15 min with 100 nM JaneliaFluor dye (JFX549 or
632 JFX646, gift from Luke Lavis, Janelia Research Campus) dissolved in imaging medium,
633 then rinsed three times with imaging medium before bathing in fresh imaging medium
634 used during imaging. Unlabeled knockin cells, unlabeled parental cells, or JFX-labeled
635 parental cells were imaged as controls to evaluate the specificity of HaloTag labeling.
636 Nuclear DNA was labeled by incubating the cells for 15 min at 37°C with SiR-DNA
637 (1:4000; Spirochrome) in imaging media during or after HaloTag labeling.
638
639 *Cell delivery and cell pairing during imaging using spinning disk confocal microscopy.*
640 1.5×10^4 SVG-A cells were seeded onto 8-well cover slips (Cellvis, C8-1.5H-N) to reach
641 30-50% confluency at the time of imaging. DMS53 cells were plated at a density of 6×10^4
642 cells/well in a 24-well plate. Cells were incubated overnight at 37°C and 5% CO_2 in DMEM
643 supplemented with 10% FBS (GeminiBio, 100-106-500) and 100 U/ml penicillin and
644 streptomycin (ThermoFisher Scientific, 15140163). The following day, plated SVG-A and
645 DMS53 cells were labeled as described above with JFX549 and JFX646 dyes,
646 respectively. For pairing, DMS53 cells were detached by incubation with PBS
647 supplemented with 0.5 mM EDTA for 3 min at 37ºC. Cells were transferred into 1.5 ml
648 microcentrifuge tubes and the PBS/EDTA solution was removed by spinning down the

649 cells for 5 min at 400-1000 *g*. The DMS53 cells were then resuspended in 200 μl imaging
650 media and 150 μl of this solution was dispensed on top of SVG-A cells plated in the 8-
651 well cover slips. 3D live spinning disk confocal imaging was then performed. Images of
652 SVG-A cells, acquired before addition of the DMS53 sender cell suspension, were used
653 as controls.
654
655 *Microfluidics device.* The microfluidics devices were fabricated as previously described
656 with some modifications (Salman et al., 2020; see Video S1). Briefly, photomasks were
657 designed with AutoCAD (AutoDesk Corp.), printed by CAD/Art Services, Inc. and placed
658 in a clean room on top of 76.2 mm silicon wafers (University Wafer, 447) to produce by
659 photolithography 60 μm depth molds using SU-8 2050 photoresist (Microchem, now
660 Kayaku Advanced Materials, Inc.). A 10:1 mixture of Sylgard 184 elastomer
661 Polydimethylsiloxane (PDMS) and curing agent (Sylgard 184 silicone elastomer kit, Dow
662 Corning) was freshly prepared, degassed for 30 min, then poured on top of the silicon
663 wafer and spin-coated at 1000 rpm for 60 s to achieve 100 μm thickness. After degassing
664 in vacuum for 10 min, the silicon wafer covered by the unpolymerized PDMS film was
665 cured by incubation at 65°C for 24 hours, after which the PDMS film was peeled off and
666 placed on top of lab tape inside a plastic petri dish. Above the sites at which the inlet /
667 outlet tubing were later attached to the device, we placed a strip of 400-700 μm thick
668 PDMS film bonded to the site using an air plasma cleaner (PDC-001 plasma cleaner,
669 Harrick Plasma) at 700 mTorr, 30 W for 1.5 min followed by incubation at 60°C for 20 min.
670 Afterwards, the PDMS film was flipped upside down and a 0.35 mm hole was punched at
671 the tubing attachment sites using a Ted Pella puncher. The chips were plasma bonded
672 to 25 mm diameter glass coverslips (CS-25R15 - 150 μm thickness, Glaswarenfabrik Karl

673 Hecht) freshly cleaned by sonication for 15 min in 1M KOH followed by 3 washes in
674 distilled water.
675
676 Tube connections to the chips were made by connecting and sealing (epoxy)
677 polyurethane tubing of 0.007" ID x 0.14" OD (BTPU-014, Instech) into Tygon tubing of
678 0.010" ID x 0.030" OD (06419-00, Cole-Parmer). The polyurethane tubing was then
679 connected to the microfluidic device and sealed with epoxy (Figure S5). Before use, the
680 microfluidic devices were sterilized by first flowing 70% ethanol through the tubing and
681 channels and then placing the device for 5 hours in 70% ethanol. Prior to cell plating, the
682 ethanol was removed by 5 sequential rinses with sterile PBS.
683
684 *Spinning disk confocal microscopy.* Cells were detached using trypsin, counted, and
685 seeded onto 8-well cover slips (Cellvis, C8-1.5H-N) in imaging media at 37°C in presence
686 of 5% CO_2 at densities chosen to reach 30-50% confluency at the time of imaging the
687 following day. Images were acquired using a Zeiss Axio-Observer Z1 (Zeiss) equipped
688 with a 63x objective (Plan-Apochromat, NA 1.4, Zeiss), a spinning disk confocal head
689 (CSU-XI, Yokogawa Electric Corporation) with additional system magnification of 1.2x,
690 and a spherical aberration correction system (Infinity Photo-Optical) controlled with a
691 Marianas system (3i, Intelligent Imaging Innovation). Volumetric images were collected
692 with 0.7 μm spacing between each optical plane and fluorescence recorded with a CCD
693 (QuantEM, 512SC, Photometrics, 0.212 x 0.212 μm/pixel in xy) or a sCMOS camera
694 (Prim 95B, Teledyne Photometrics, 0.145 x 0.145 μm/pixel in xy). The fluorophores were
695 excited using solid-state lasers (Coherent Inc.) with λ excitation at 488, 561, or 640 nm
696 coupled to an acoustic-optical tunable filter or the LaserStack (3i, Intelligent Imaging
697 Innovation) using solid state diode lasers coupled through single mode optical fibers to

698 the LaserStream™ (3i, Intelligent Imaging Innovation). With the CCD camera, exposure
699 times of 100 ms in all channels were used to image membranes, Notch synapses, and
700 nuclei; exposure times of 50 ms were used to image vesicles. With the sCMOS camera,
701 exposure times of 60 ms were used to image signals in the 561 and 640 nm channels,
702 exposure times of 100 ms were used in the 488 nm channel to image cell nuclei, and
703 exposure times of 50 ms (488 nm channel), 30 ms (561 nm channel), and 60 ms (640 nm
704 channel) were used to image vesicles.
705
706 *Lattice light-sheet microscopy modified with adaptive optics (MOSAIC).* Time-lapse live
707 3D z-stacks were acquired using a lattice light-sheet microscope modified with adaptive
708 optics, referred here as MOSAIC (Multimodal Optical Scope with Adaptive Imaging
709 Correction). Live cell volumetric imaging was achieved by acquiring single time points at
710 1 min intervals for 1 hour or longer. Sequential images spaced 0.40 μm between each
711 plane along the z-imaging axis were obtained in sample scan mode; each time point
712 consisted of z-stack comprised of 90-200 z-planes. Samples were illuminated with a
713 dithered multi-Bessel lattice light-sheet (Chen et al., 2014) with 0.50 inner and 0.55 outer
714 numerical apertures (NA) of the annular mask; lasers (MPB Communications Inc.)
715 emitting at 488, 560 or 642 nm were used for illumination. A 0.65 NA (Special Optics) and
716 a 1.0 NA objective (Zeiss) were used for illumination and detection using sCMOS
717 cameras (Hamamatsu, ORCA Flash 4.0 v3) with 0.104 x 0.104 μm/pixel in xy for data
718 visualization. Typical exposures were 50 ms for 488 nm (mNeonGreen – N2-N), 20 ms
719 for 560 nm (HaloTag labeled with JFX549 – N2-C), and 20 ms for 642 nm (SiR-DNA or
720 HaloTag labelled with JFX646 – DLL4).
721

722 *Cell delivery and cell pairing during imaging using MOSAIC.* $1.5x10^5$ SVG-A cells were
723 plated onto the center of the microfluidics device, followed by overnight incubation at 37°C
724 and 5% CO_2 in DMEM supplemented with 10% fetal bovine serum (FBS, GeminiBio, 100-
725 106-500) and 100 U/ml penicillin and streptomycin (ThermoFisher Scientific, 15140163).
726 Prior to imaging, the cells were labeled as described. The microfluidics device with
727 attached SVG-A cells was then placed on the MOSAIC sample holder and its inlet tubing
728 (Tygon tubing 0.010" ID x 0.030" OD (06419-00, Cole-Parmer)) was connected to the flow
729 meter (Flow Unit M Flow-Rate Platform, Fluigent) (Figure S5). Another tubing, connected
730 to a 2 ml microcentrifuge tube (Eppendorf) with an air-tight metal tube cap (P-CAP 2 mL
731 High Pressure, Fluigent) containing a suspension of $5x10^5$ DMS53 cells labeled with
732 JFX646, was also connected to the inlet of the flow meter. The sealed tube was further
733 connected to the pressure controller (Microfluidic Flow Control System – EZ, Fluigent)
734 using pneumatic tubing. The tube with suspended DMS53 cells was kept up to 5 min at
735 37°C (dry bath, My Block, Benchmark) before cell injection into the microfluidics device.
736 Inlet pressure of 50-100 mbar and a flow of 10-15 μl/min for 30-90 s of the suspension
737 containing DMS53 sender cells were controlled in real time using MAESFLO software
738 (Fluigent). Upon ending the flow, the DMS53 cells were allowed to settle by gravity and
739 to pair with the SVG-A cells attached in the microfluidics device.
740
741 *Fluorescence recovery after photobleaching (FRAP).* Fluorescence recovery after
742 photobleaching (FRAP) was performed with the spinning disk confocal microscope by
743 photobleaching a region of interest (ROI) of 1 μm in radius for 5 ms using 100% laser
744 power. A 100 ms exposure time was used to collect images every 1 s for 10 s before
745 bleaching and for 60 s after bleaching. SVG-A and DMS53 cells, alone or in pairs were
746 used to perform single FRAP experiments for a given isolated cell or cell-pair. For

747 photobleaching of synapses, 1-2 ROI were selected on the Notch synapse, while another
748 ROI elsewhere on the cell membrane was used as a control. The position of the synapse
749 within the ROI was determined by imaging in a non-bleached channel. A similar time
750 series acquired in a different region of the cell not subjected to FRAP was used to correct
751 for bleaching due to imaging only.

752 **Data analysis**

753

754 *Ratiometric analysis.* The relative amounts of N2-N (mNeonGreen), N2-C (HaloTag) and
755 DLL4 (HaloTag) or JAG1 (HaloTag) associated with the Notch synapse, excluded from it
756 and in the cell membrane, or associated with vesicles in the sender cell were determined
757 by ratiometric analysis of the corresponding fluorescence signals within appropriate ROIs.
758 The first step in the ratiometric analysis consisted in determining the relative amount of
759 N2-N, N2-C and DLL4 (or JAG1) within a given image. This step was achieved by
760 comparing the fluorescence intensity of N2-N with respect to N2-C ($HaloTag^{JFX549}$) or N2-
761 N with respect to DLL4 ($HaloTag^{JFX549}$) or JAG1 ($HaloTag^{JFX549}$). The second step
762 established the relative signal resulting from JFX549 and JFX646 labeling by comparing
763 the relative fluorescence intensity of N2-C ($HaloTag^{JFX549}$) in one sample with respect to
764 N2-C ($HaloTag^{JFX646}$) in a second independently labeled sample.
765 Ratiometric analysis of fluorescence signals within appropriate ROIs was performed by
766 using a Macro written for Fiji (Schindelin et al., 2012). A three-pixel width line was drawn
767 across the membrane or synapse as an ROI to obtain the mean fluorescence intensity
768 (F.I.) of the measured values within the line width. To account for the three dimensionality,
769 two planes below and two planes above the ROI were determined, resulting in 5 ROI, one
770 per plane. The maximum intensity F.I. in those 5 ROI (usually coincident with the main
771 ROI) was subtracted by the F.I. of the background to obtain the $F.I.^{max}$, a value
772 proportional to the density of molecules at the Notch synapse, on the surrounding cell
773 membrane surface, and in vesicles within the sender cell.
774 The ratiometric quantification of N2-N associated with intracellular vesicles in the DMS53
775 sender cell was corrected by the intrinsic autofluorescence $F.I.^{af}$, determined in unpaired

776 DMS53 cells imaged in the microfluidics device 60 minutes after initiation of the cell
777 pairing experiment.
778

779 *FRAP analysis.* FRAP analysis was conducted as described (Govindaraj & Post, 2021)
780 using Fiji (Schindelin et al., 2012) on the fluorescent signal within the photobleached ROI
781 of the Notch synapse or plasma membrane after correcting the fluorescent signals for the
782 inherent photobleaching due to imaging; the fluorescence intensity of the first 10 time
783 points prior to FRAP were averaged and normalized to 1. The FRAP recovery curve was
784 fitted using a single decay exponential from which the diffusion coefficient was estimated
785 as $D = (0.224 \times r^2)/ t_{1/2}$, where r is the radius of the bleached ROI and $t_{1/2}$ the half-life of
786 recovery (Kang et al., 2012).
787

788 *Nuclear N2-C (i.e. NICD) concentration.* The nuclear N2-C (*i.e.* NICD) concentration was
789 estimated by applying the volume calibration curve to the mean nuclear NICD
790 fluorescence intensity (F.I.) from the non-punctate and diffuse nuclear N2-C signal. A
791 macro written using Fiji (Schindelin et al., 2012) was used to automate the calculations.
792 A binary mask of the nucleus defined by the SiR-DNA signal from Notch cells was used
793 to define the nuclear region from which to calculate the averaged intensity per plane; an
794 estimate of the nuclear volume was obtained by multiplying the z-planes by the space
795 between optical planes (0.7 μm). The extent of out of focus fluorescence contributed by
796 molecules located on the plasma membrane to different z-planes within the nucleus was
797 estimated by measuring the fluorescence of N2-C (*i.e.* NECD; which is always absent
798 from the nucleus). This value was then used to correct for the contribution of out of plane
799 N2-C signal from the plasma membrane to the nuclear signal value.
800

801 *Nuclear N2-C (i.e. NICD) concentration, N2-N molecules in synapse and in DMS53 cell*
802 *vesicles in the time-lapse 3D z-stacks acquired using MOSAIC.* The fluorescence signals
803 obtained with MOSAIC were normalized to the signals obtained with the SD. This
804 normalization was done by determining the ratio of N2-C (HaloTag^{JFX549}) fluorescence
805 within a plane orthogonal to the plasma membrane acquired with MOSAIC and SD. The
806 nuclear N2-C concentration was estimated as above using SD.
807 A binary mask corresponding to the Notch synapse was defined by the logical intersection
808 of the N2-N, N2-C and DLL4 signals. The averaged N2-N fluorescence signal per pixel
809 (0.1x0.1x0.4 µm) times the number of pixels corrected by N2-N membrane signal outside
810 of the synapse and normalized by the signal ratio between N2-N and N2-C on the
811 membrane corresponds to the number of N2-N (*i.e.* NECD) molecules in the synapse.
812 Vesicles containing N2-N in DLL4 cells were identified using the 3D cmeAnalysis software
813 (Aguet et al., 2016). The volume of a given vesicle was defined as a box of 3x3x3 (x,y,z)
814 pixels from which the N2-N average fluorescence and the number of molecules per
815 vesicle were calculated as described above. This number multiplied by the number of
816 vesicles corresponded to the total amount of N2-N transendocytosis into the DLL4 cell.
817
818 *Statistical analysis.* All statistical analyses were performed using GraphPad Prism
819 (GraphPad). Sample distribution and normality tests were performed for each data set.
820 Statistical tests that were used are indicated in the figure legends.
821
822 *Data and code availability.* Raw data, MATLAB codes, and FIJI macros are available upon
823 request. RNA-Seq data is accessible at NCBI GEO database (Edgar et al., 2002)
824 accession GSE235637.

825 **References**

826

827 Agrawal, N., Frederick, M. J., Pickering, C. R., Bettegowda, C., Chang, K., Li, R. J.,
828 Fakhry, C., Xie, T.-X., Zhang, J., Wang, J., Zhang, N., El-Naggar, A. K., Jasser, S.
829 A., Weinstein, J. N., Treviño, L., Drummond, J. A., Muzny, D. M., Wu, Y., Wood,
830 L. D., … Myers, J. N. (2011). Exome sequencing of head and neck squamous cell
831 carcinoma reveals inactivating mutations in NOTCH1. *Science*, *333*(6046), 1154–
832 1157. https://doi.org/10.1126/science.1206923

833 Aguet, F., Upadhyayula, S., Gaudin, R., Chou, Y. Y., Cocucci, E., He, K., Chen, B. C.,
834 Mosaliganti, K., Pasham, M., Skillern, W., Legant, W. R., Liu, T. L., Findlay, G.,
835 Marino, E., Danuser, G., Megason, S., Betzig, E., & Kirchhausen, T. (2016).
836 Membrane dynamics of dividing cells imaged by lattice light-sheet microscopy.
837 *Molecular Biology of the Cell*, *27*(22), 3418–3435.
838 https://doi.org/10.1091/mbc.E16-03-0164

839 Allgood, A. G., & Barrick, D. (2011). Mapping the Deltex-binding surface on the notch
840 ankyrin domain using analytical ultracentrifugation. *Journal of Molecular Biology*,
841 *414*(2), 243–259. https://doi.org/10.1016/j.jmb.2011.09.050

842 Arnett, K. L., Hass, M., McArthur, D. G., Ilagan, M. X. G., Aster, J. C., Kopan, R., &
843 Blacklow, S. C. (2010). Structural and mechanistic insights into cooperative
844 assembly of dimeric Notch transcription complexes. *Nature Structural & Molecular*
845 *Biology*, *17*(11), 1312–1317. https://doi.org/10.1038/nsmb.1938

846 Artavanis-Tsakonas, S., Muskavitcht, M. A. T., & Yedvobnick, B. (1983). Molecular
847 cloning of Notch, a locus affecting neurogenesis in Drosophila melanogaster.
848 *Genetics*, *80*, 1977–1981.

849 Aster, J. C., Pear, W. S., & Blacklow, S. C. (2017). The varied roles of Notch in cancer.
850 *Annual Review of Pathology*, *12*, 245–275. https://doi.org/10.1146/annurev-pathol-
851 052016-100127
852 Blaumueller, C. M., Qi, H., Zagouras, P., & Artavanis-Tsakonas, S. (1997). Intracellular
853 cleavage of Notch leads to a heterodimeric receptor on the plasma membrane.
854 *Cell*, *90*(2), 281–291. https://doi.org/10.1016/s0092-8674(00)80336-0
855 Bray, S. J. (2016). Notch signalling in context. *Nature Reviews. Molecular Cell Biology*,
856 *17*(11), 722–735. https://doi.org/10.1038/nrm.2016.94
857 Chapman, G., Major, J. A., Iyer, K., James, A. C., Pursglove, S. E., Moreau, J. L. M., &
858 Dunwoodie, S. L. (2016). Notch1 endocytosis is induced by ligand and is required
859 for signal transduction. *Biochimica et Biophysica Acta*, *1863*(1), 166–177.
860 https://doi.org/10.1016/j.bbamcr.2015.10.021
861 Chapman, G., Sparrow, D. B., Kremmer, E., & Dunwoodie, S. L. (2011). Notch inhibition
862 by the ligand DELTA-LIKE 3 defines the mechanism of abnormal vertebral
863 segmentation in spondylocostal dysostosis. *Human Molecular Genetics*, *20*(5),
864 905–916. https://doi.org/10.1093/hmg/ddq529
865 Chastagner, P., Rubinstein, E., & Brou, C. (2017). Ligand-activated Notch undergoes
866 DTX4-mediated ubiquitylation and bilateral endocytosis before ADAM10
867 processing. *Science Signaling*, *10*(483), 1–14.
868 https://doi.org/10.1126/scisignal.aag2989
869 Chen, B.-C., Legant, W. R., Wang, K., Shao, L., Milkie, D. E., Davidson, M. W.,
870 Janetopoulos, C., Wu, X. S., Hammerv, J. A., Iii, Liu, Z., English, B. P., Mimori-
871 Kiyosue, Y., Romero, D. P., Ritter, A. T., Lippincott-Schwartz, J., Fritz-Laylin, L.,
872 Mullins, R. D., Mitchell, D. M., Bembenek, J. N., … Betzig, E. (2014). Lattice Light
873 Sheet Microscopy: Imaging Molecules to Embryos at High Spatiotemporal

874 Resolution Bi-Chang. *Science*, *346*(6208).
875 https://doi.org/10.1126/science.1257998.Lattice
876 Chen, E. Y., Tan, C. M., Kou, Y., Duan, Q., Wang, Z., Meirelles, G. V., Clark, N. R., &
877 Ma'ayan, A. (2013). Enrichr: interactive and collaborative HTML5 gene list
878 enrichment analysis tool. *BMC Bioinformatics*, *14*, 128.
879 https://doi.org/10.1186/1471-2105-14-128
880 Chou, Y.-Y., Krupp, A., Kaynor, C., Gaudin, R., Ma, M., Cahir-McFarland, E., &
881 Kirchhausen, T. (2016). Inhibition of JCPyV infection mediated by targeted viral
882 genome editing using CRISPR/Cas9. *Scientific Reports*, *6*, 36921.
883 https://doi.org/10.1038/srep36921
884 Couturier, L., Vodovar, N., & Schweisguth, F. (2012). Endocytosis by Numb breaks Notch
885 symmetry at cytokinesis. *Nature Cell Biology*, *14*(2), 131–139.
886 https://doi.org/10.1038/ncb2419
887 Daskalaki, A., Shalaby, N. A., Kux, K., Tsoumpekos, G., Tsibidis, G. D., Muskavitch, M.
888 A. T., & Delidakis, C. (2011). Distinct intracellular motifs of Delta mediate its
889 ubiquitylation and activation by Mindbomb1 and Neuralized. *The Journal of Cell*
890 *Biology*, *195*(6), 1017–1031. https://doi.org/10.1083/jcb.201105166
891 Dobin, A., Davis, C. A., Schlesinger, F., Drenkow, J., Zaleski, C., Jha, S., Batut, P.,
892 Chaisson, M., & Gingeras, T. R. (2012). STAR: ultrafast universal RNA-seq
893 aligner. *Bioinformatics* , *29*(1), 15–21.
894 https://doi.org/10.1093/bioinformatics/bts635
895 Edgar, R., Domrachev, M., & Lash, A. E. (2002). Gene Expression Omnibus: NCBI gene
896 expression and hybridization array data repository. *Nucleic Acids Research*, *30*(1),
897 207–210. https://doi.org/10.1093/nar/30.1.207

898 Falo-Sanjuan, J., & Bray, S. (2022). Notch-dependent and -independent transcription are
899 modulated by tissue movements at gastrulation. In *eLife* (Vol. 11).
900 https://doi.org/10.7554/elife.73656
901 Falo-Sanjuan, J., Lammers, N. C., Garcia, H. G., & Bray, S. J. (2019). Enhancer Priming
902 Enables Fast and Sustained Transcriptional Responses to Notch Signaling.
903 *Developmental Cell*, *50*(4), 411-425.e8.
904 https://doi.org/10.1016/j.devcel.2019.07.002
905 Fehon, R. G., Kooh, P. J., Rebay, I., Regan, C. L., Xu, T., Muskavitch, M. A., & Artavanis-
906 Tsakonas, S. (1990). Molecular interactions between the protein products of the
907 neurogenic loci Notch and Delta, two EGF-homologous genes in Drosophila. *Cell*,
908 *61*(3), 523–534. https://doi.org/10.1016/0092-8674(90)90534-l
909 Gordon, W. R., Roy, M., Vardar-Ulu, D., Garfinkel, M., Mansour, M. R., Aster, J. C., &
910 Blacklow, S. C. (2009). Structure of the Notch1-negative regulatory region:
911 Implications for normal activation and pathogenic signaling in T-ALL. *Blood*,
912 *113*(18), 4381–4390. https://doi.org/10.1182/blood-2008-08-174748
913 Gordon, W. R., Vardar-Ulu, D., Histen, G., Sanchez-Irizarry, C., Aster, J. C., & Blacklow,
914 S. C. (2007). Structural basis for autoinhibition of Notch. *Nature Structural &*
915 *Molecular Biology*, *14*(4), 295–300. https://doi.org/10.1038/nsmb1227
916 Govindaraj, K., & Post, J. N. (2021). Using FRAP to Quantify Changes in Transcription
917 Factor Dynamics After Cell Stimulation: Cell Culture, FRAP, Data Analysis, and
918 Visualization. *Methods in Molecular Biology* , *2221*, 109–139.
919 https://doi.org/10.1007/978-1-0716-0989-7_9
920 Grimm, J. B., Xie, L., Casler, J. C., Patel, R., Tkachuk, A. N., Choi, H., Lippincott-
921 Schwartz, J., Brown, T. A., Glick, B. S., Liu, Z., & Lavis, L. D. (2020). Deuteration

922 improves small-molecule fluorophores. In *bioRxiv* (p. 2020.08.17.250027).
923 https://doi.org/10.1101/2020.08.17.250027
924 Guo, B., McMillan, B. J., & Blacklow, S. C. (2016). Structure and function of the Mind
925 bomb E3 ligase in the context of Notch signal transduction. *Current Opinion in*
926 *Structural Biology*, *41*, 38–45. https://doi.org/10.1016/j.sbi.2016.05.012
927 Ilagan, M. X. G., Lim, S., Fulbright, M., Piwnica-Worms, D., & Kopan, R. (2011). Real-
928 time imaging of Notch activation with a luciferase complementation-based
929 reporter. *Science Signaling*, *4*(181), 1–15.
930 https://doi.org/10.1126/scisignal.2001656
931 Jacobson, K., Ishihara, A., & Inman, R. (1987). Lateral diffusion of proteins in membranes.
932 *Annual Review of Physiology*, *49*, 163–175.
933 https://doi.org/10.1146/annurev.ph.49.030187.001115
934 Joutel, A., Corpechot, C., Ducros, A., Vahedi, K., Chabriat, H., Mouton, P., Alamowitch,
935 S., Domenga, V., Cécillion, M., Marechal, E., Maciazek, J., Vayssiere, C., Cruaud,
936 C., Cabanis, E. A., Ruchoux, M. M., Weissenbach, J., Bach, J. F., Bousser, M. G.,
937 & Tournier-Lasserve, E. (1996). Notch3 mutations in CADASIL, a hereditary adult-
938 onset condition causing stroke and dementia. *Nature*, *383*(6602), 707–710.
939 https://doi.org/10.1038/383707a0
940 Kamath, B. M., Bauer, R. C., Loomes, K. M., Chao, G., Gerfen, J., Hutchinson, A.,
941 Hardikar, W., Hirschfield, G., Jara, P., Krantz, I. D., Lapunzina, P., Leonard, L.,
942 Ling, S., Ng, V. L., Hoang, P. L., Piccoli, D. A., & Spinner, N. B. (2012). NOTCH2
943 mutations in Alagille syndrome. *Journal of Medical Genetics*, *49*(2), 138–144.
944 https://doi.org/10.1136/jmedgenet-2011-100544

Kang, M., Day, C. A., Kenworthy, A. K., & DiBenedetto, E. (2012). Simplified equation to extract diffusion coefficients from confocal FRAP data. *Traffic* , *13*(12), 1589–1600. https://doi.org/10.1111/tra.12008

Khait, I., Orsher, Y., Golan, O., Binshtok, U., Gordon-Bar, N., Amir-Zilberstein, L., & Sprinzak, D. (2016). Quantitative Analysis of Delta-like 1 Membrane Dynamics Elucidates the Role of Contact Geometry on Notch Signaling. *Cell Reports*, *14*(2), 225–233. https://doi.org/10.1016/j.celrep.2015.12.040

Khamaisi, B., Luca, V. C., Blacklow, S. C., & Sprinzak, D. (2022). Functional Comparison between Endogenous and Synthetic Notch Systems. *ACS Synthetic Biology*, *11*(10), 3343–3353. https://doi.org/10.1021/acssynbio.2c00247

Klueg, K. M., & Muskavitch, M. a. (1999). Ligand-receptor interactions and trans-endocytosis of Delta, Serrate and Notch: members of the Notch signalling pathway in Drosophila. *Journal of Cell Science*, *112 (Pt 19)*, 3289–3297. https://doi.org/10.1038/ncb0609-678

Kovall, R. A., Gebelein, B., Sprinzak, D., & Kopan, R. (2017). The Canonical Notch Signaling Pathway: Structural and Biochemical Insights into Shape, Sugar, and Force. *Developmental Cell*, *41*(3), 228–241. https://doi.org/10.1016/j.devcel.2017.04.001

Kuleshov, M. V., Jones, M. R., Rouillard, A. D., Fernandez, N. F., Duan, Q., Wang, Z., Koplev, S., Jenkins, S. L., Jagodnik, K. M., Lachmann, A., McDermott, M. G., Monteiro, C. D., Gundersen, G. W., & Ma'ayan, A. (2016). Enrichr: a comprehensive gene set enrichment analysis web server 2016 update. *Nucleic Acids Research*, *44*(W1), W90-7. https://doi.org/10.1093/nar/gkw377

968 Kurooka, H., Kuroda, K., & Honjo, T. (1998). Roles of the ankyrin repeats and C-terminal
969 region of the mouse Notch1 intracellular region. *Nucleic Acids Research*, *26*(23),
970 5448–5455. https://doi.org/10.1093/nar/26.23.5448
971 Langmead, B., Trapnell, C., Pop, M., & Salzberg, S. L. (2009). Ultrafast and memory-
972 efficient alignment of short DNA sequences to the human genome. *Genome*
973 *Biology*, *10*(3), R25. https://doi.org/10.1186/gb-2009-10-3-r25
974 Langridge, P. D., & Struhl, G. (2017). Epsin-Dependent Ligand Endocytosis Activates
975 Notch by Force. *Cell*, *171*(6), 1383-1396.e12.
976 https://doi.org/10.1016/j.cell.2017.10.048
977 Li, L., Krantz, I. D., Deng, Y., Genin, A., Banta, A. B., Collins, C. C., Qi, M., Trask, B. J.,
978 Kuo, W. L., Cochran, J., Costa, T., Pierpont, M. E., Rand, E. B., Piccoli, D. A.,
979 Hood, L., & Spinner, N. B. (1997). Alagille syndrome is caused by mutations in
980 human Jagged1, which encodes a ligand for Notch1. *Nature Genetics*, *16*(3), 243–
981 251. https://doi.org/10.1038/ng0797-243
982 Liao, Y., Smyth, G. K., & Shi, W. (2013). featureCounts: an efficient general purpose
983 program for assigning sequence reads to genomic features. *Bioinformatics* , *30*(7),
984 923–930. https://doi.org/10.1093/bioinformatics/btt656
985 Logeat, F., Bessia, C., Brou, C., LeBail, O., Jarriault, S., Seidah, N. G., & Israël, A. (1998).
986 The Notch1 receptor is cleaved constitutively by a furin-like convertase.
987 *Proceedings of the National Academy of Sciences of the United States of America*,
988 *95*(14), 8108–8112. https://doi.org/10.1073/pnas.95.14.8108
989 Los, G. V., Encell, L. P., McDougall, M. G., Hartzell, D. D., Karassina, N., Zimprich, C.,
990 Wood, M. G., Learish, R., Ohana, R. F., Urh, M., Simpson, D., Mendez, J.,
991 Zimmerman, K., Otto, P., Vidugiris, G., Zhu, J., Darzins, A., Klaubert, D. H., Bulleit,
992 R. F., & Wood, K. V. (2008). HaloTag: a novel protein labeling technology for cell

993 imaging and protein analysis. *ACS Chemical Biology*, *3*(6), 373–382.
994 https://doi.org/10.1021/cb800025k
995 Love, M. I., Huber, W., & Anders, S. (2014). Moderated estimation of fold change and
996 dispersion for RNA-seq data with DESeq2. *Genome Biology*, *15*(12), 550.
997 https://doi.org/10.1186/s13059-014-0550-8
998 Malecki, M. J., Sanchez-Irizarry, C., Mitchell, J. L., Histen, G., Xu, M. L., Aster, J. C., &
999 Blacklow, S. C. (2006). Leukemia-associated mutations within the NOTCH1
1000 heterodimerization domain fall into at least two distinct mechanistic classes.
1001 *Molecular and Cellular Biology*, *26*(12), 4642–4651.
1002 https://doi.org/10.1128/MCB.01655-05
1003 Martin, A. P., Bradshaw, G. A., Eisert, R. J., Egan, E. D., Tveriakhina, L., Rogers, J. M.,
1004 Dates, A. N., Scanavachi, G., Aster, J. C., Kirchhausen, T., Kalocsay, M., &
1005 Blacklow, S. C. (2023). A spatiotemporal Notch interaction map from plasma
1006 membrane to nucleus. *Science Signaling*, *16*(796), eadg6474.
1007 https://doi.org/10.1126/scisignal.adg6474
1008 Martincorena, I., Roshan, A., Gerstung, M., Ellis, P., Van Loo, P., McLaren, S., Wedge,
1009 D. C., Fullam, A., Alexandrov, L. B., Tubio, J. M., Stebbings, L., Menzies, A.,
1010 Widaa, S., Stratton, M. R., Jones, P. H., & Campbell, P. J. (2015). Tumor evolution.
1011 High burden and pervasive positive selection of somatic mutations in normal
1012 human skin. *Science*, *348*(6237), 880–886.
1013 https://doi.org/10.1126/science.aaa6806
1014 McMillan, B. J., Schnute, B., Ohlenhard, N., Zimmerman, B., Miles, L., Beglova, N., Klein,
1015 T., & Blacklow, S. C. (2015). A Tail of Two Sites: A Bipartite Mechanism for
1016 Recognition of Notch Ligands by Mind Bomb E3 Ligases. *Molecular Cell*, *57*(5),
1017 912–924. https://doi.org/10.1016/j.molcel.2015.01.019

1018 Meloty-Kapella, L., Shergill, B., Kuon, J., Botvinick, E., & Weinmaster, G. (2012). Notch
1019 ligand endocytosis generates mechanical pulling force dependent on dynamin,
1020 epsins, and actin. *Developmental Cell*, *22*(6), 1299–1312.
1021 https://doi.org/10.1016/j.devcel.2012.04.005
1022 Minoguchi, S., Taniguchi, Y., Kato, H., Okazaki, T., Strobl, L. J., Zimber-Strobl, U.,
1023 Bornkamm, G. W., & Honjo, T. (1997). RBP-L, a transcription factor related to RBP-
1024 Jkappa. *Molecular and Cellular Biology*, *17*(5), 2679–2687.
1025 https://doi.org/10.1128/MCB.17.5.2679
1026 Mumm, J. S., Schroeter, E. H., Saxena, M. T., Griesemer, A., Tian, X., Pan, D. J., Ray,
1027 W. J., & Kopan, R. (2000). A ligand-induced extracellular cleavage regulates
1028 gamma-secretase-like proteolytic activation of Notch1. *Molecular Cell*, *5*(2), 197–
1029 206. https://doi.org/10.1016/S1097-2765(00)80416-5
1030 Nichols, J. T., Miyamoto, A., Olsen, S. L., D'Souza, B., Yao, C., & Weinmaster, G. (2007).
1031 DSL ligand endocytosis physically dissociates Notch1 heterodimers before
1032 activating proteolysis can occur. *The Journal of Cell Biology*, *176*(4), 445–458.
1033 https://doi.org/10.1083/jcb.200609014
1034 Oda, T., Elkahloun, A. G., Pike, B. L., Okajima, K., Krantz, I. D., Genin, A., Piccoli, D. A.,
1035 Meltzer, P. S., Spinner, N. B., Collins, F. S., & Chandrasekharappa, S. C. (1997).
1036 Mutations in the human Jagged1 gene are responsible for Alagille syndrome.
1037 *Nature Genetics*, *16*(3), 235–242. https://doi.org/10.1038/ng0797-235
1038 Okano, M., Matsuo, H., Nishimura, Y., Hozumi, K., Yoshioka, S., Tonoki, A., & Itoh, M.
1039 (2016). Mib1 modulates dynamin 2 recruitment via Snx18 to promote Dll1
1040 endocytosis for efficient Notch signaling. *Genes to Cells: Devoted to Molecular &*
1041 *Cellular Mechanisms*, *21*(5), 425–441. https://doi.org/10.1111/gtc.12350

1042 Parks, A. L., Klueg, K. M., Stout, J. R., & Muskavitch, M. A. (2000). Ligand endocytosis
1043 drives receptor dissociation and activation in the Notch pathway. *Development* ,
1044 *127*(7), 1373–1385. https://doi.org/10.1242/dev.127.7.1373
1045 Pillidge, Z., & Bray, S. J. (2019). SWI/SNF chromatin remodeling controls Notch-
1046 responsive enhancer accessibility. *EMBO Reports*, *20*(5), e46944.
1047 https://doi.org/10.15252/embr.201846944
1048 Puente, X. S., Pinyol, M., Quesada, V., Conde, L., Ordóñez, G. R., Villamor, N.,
1049 Escaramis, G., Jares, P., Beà, S., González-Díaz, M., Bassaganyas, L., Baumann,
1050 T., Juan, M., López-Guerra, M., Colomer, D., Tubío, J. M. C., López, C., Navarro,
1051 A., Tornador, C., … Campo, E. (2011). Whole-genome sequencing identifies
1052 recurrent mutations in chronic lymphocytic leukaemia. *Nature*, *475*(7354), 101–
1053 105. https://doi.org/10.1038/nature10113
1054 Salman, M. M., Marsh, G., Kusters, I., Delincé, M., Di Caprio, G., Upadhyayula, S., de
1055 Nola, G., Hunt, R., Ohashi, K. G., Gray, T., Shimizu, F., Sano, Y., Kanda, T.,
1056 Obermeier, B., & Kirchhausen, T. (2020). Design and Validation of a Human Brain
1057 Endothelial Microvessel-on-a-Chip Open Microfluidic Model Enabling Advanced
1058 Optical Imaging. *Frontiers in Bioengineering and Biotechnology*, *8*, 573775.
1059 https://doi.org/10.3389/fbioe.2020.573775
1060 Schindelin, J., Arganda-Carreras, I., Frise, E., Kaynig, V., Longair, M., Pietzsch, T.,
1061 Preibisch, S., Rueden, C., Saalfeld, S., Schmid, B., Tinevez, J.-Y., White, D. J.,
1062 Hartenstein, V., Eliceiri, K., Tomancak, P., & Cardona, A. (2012). Fiji: an open-
1063 source platform for biological-image analysis. *Nature Methods*, *9*(7), 676–682.
1064 https://doi.org/10.1038/nmeth.2019
1065 Shaner, N. C., Lambert, G. G., Chammas, A., Ni, Y., Cranfill, P. J., Baird, M. A., Sell, B.
1066 R., Allen, J. R., Day, R. N., Israelsson, M., Davidson, M. W., & Wang, J. (2013). A

1067 bright monomeric green fluorescent protein derived from Branchiostoma
1068 lanceolatum. *Nature Methods*, *10*(5), 407–409.
1069 https://doi.org/10.1038/nmeth.2413
1070 Sprinzak, D., & Blacklow, S. C. (2021). Biophysics of Notch Signaling. *Annual Review of*
1071 *Biophysics*. https://doi.org/10.1146/annurev-biophys-101920-082204
1072 van Tetering, G., van Diest, P., Verlaan, I., van der Wall, E., Kopan, R., & Vooijs, M.
1073 (2009). Metalloprotease ADAM10 is required for Notch1 site 2 cleavage. *The*
1074 *Journal of Biological Chemistry*, *284*(45), 31018–31027.
1075 https://doi.org/10.1074/jbc.M109.006775
1076 Wang, N. J., Sanborn, Z., Arnett, K. L., Bayston, L. J., Liao, W., Proby, C. M., Leigh, I. M.,
1077 Collisson, E. A., Gordon, P. B., Jakkula, L., Pennypacker, S., Zou, Y., Sharma, M.,
1078 North, J. P., Vemula, S. S., Mauro, T. M., Neuhaus, I. M., Leboit, P. E., Hur, J. S.,
1079 … Cho, R. J. (2011). Loss-of-function mutations in Notch receptors in cutaneous
1080 and lung squamous cell carcinoma. *Proceedings of the National Academy of*
1081 *Sciences of the United States of America*, *108*(43), 17761–17766.
1082 https://doi.org/10.1073/pnas.1114669108
1083 Weng, A. P., Ferrando, A. A., Lee, W., Morris, J. P., 4th, Silverman, L. B., Sanchez-
1084 Irizarry, C., Blacklow, S. C., Look, A. T., & Aster, J. C. (2004). Activating mutations
1085 of NOTCH1 in human T cell acute lymphoblastic leukemia. *Science*, *306*(5694),
1086 269–271. https://doi.org/10.1126/science.1102160
1087 Wilhelm, J., Kühn, S., Tarnawski, M., Gotthard, G., Tünnermann, J., Tänzer, T.,
1088 Karpenko, J., Mertes, N., Xue, L., Uhrig, U., Reinstein, J., Hiblot, J., & Johnsson,
1089 K. (2021). Kinetic and Structural Characterization of the Self-Labeling Protein Tags
1090 HaloTag7, SNAP-tag, and CLIP-tag. *Biochemistry*, *60*(33), 2560–2575.
1091 https://doi.org/10.1021/acs.biochem.1c00258

1092 Xu, X., Choi, S. H., Hu, T., Tiyanont, K., Habets, R., Groot, A. J., Vooijs, M., Aster, J. C.,
1093 Chopra, R., Fryer, C., & Blacklow, S. C. (2015). Insights into Autoregulation of
1094 Notch3 from Structural and Functional Studies of Its Negative Regulatory Region.
1095 *Structure* , *23*(7), 1227–1235. https://doi.org/10.1016/j.str.2015.05.001
1096

1097 **Figure legends**

1098

1099 **Figure 1. Formation of synapses at sites of NOTCH2-DLL4 contact. A.** Domain
1100 organization of NOTCH2 and DLL4. The NOTCH2 extracellular domain (N2-N) is green,
1101 the NOTCH2 transmembrane subunit (N2-C) is magenta, and DLL4 is blue. N- and C-
1102 terminal tagging sites are shown in black. The sites of NOTCH2 proteolytic cleavage by
1103 Furin (S1), ADAM10 (S2), and γ-secretase (S3) are also indicated. **B.** Schematic showing
1104 the colors of the fluorescent labels used in cell pairing experiments. The N2-N label on
1105 NECD is mNeonGreen, the N2-C label on the C-terminal tail of NOTCH2 is HaloTag
1106 coupled to JFX549 (magenta), and the DLL4 C-terminal label is HaloTag coupled to a
1107 JFX646 (blue). **C.** Schematic of the cell paring procedure. NOTCH2 and DLL4 cells were
1108 separately labeled with JFX549 and JFX646. DLL4 cells were detached and delivered to
1109 NOTCH2 cells, and cell pairing was monitored by spinning disk confocal or lattice light-
1110 sheet microscopy. **D.** Representative lattice light-sheet images (orthogonal view,
1111 despeckle) showing NOTCH2 cells before (0 min) and 1, 3, and 5 min after microfluidic
1112 delivery of DLL4 cells. N2-N is colored green, N2-C is magenta, DLL4 is cyan, and DNA
1113 is pseudocolored blue. The synapse is indicated with a yellow arrowhead. **E.**
1114 Fluorescence intensities of N2-N, N2-C, and DLL4 signals in the regions outside of cell-
1115 cell contact (membrane) and in synapses. **F**. Ratios of fluorescence intensities of signals
1116 associated with N2-N and N2-C in the membrane and of N2-N and N2-C or N2-N and
1117 DLL4 in synapses, respectively. Data are represented as mean ± standard deviation;
1118 statistical analysis for each pair in **E** was performed using Mann-Whitney test and in **F**
1119 using Kruskal-Wallis one-way ANOVA; **** = $p<0.0001$, ns = $p>0.05$; n = number of
1120 synapses and number of cells analyzed as indicated.

1121

1122 **Figure 2. NOTCH2 and DLL4 in synapses do not readily exchange. A.** Fluorescence
1123 recovery after photobleaching (FRAP) experiment, showing representative spinning disk
1124 confocal images of N2-N, N2-C, and DLL4 freely dispersed in the membrane before and
1125 as a function of time after photobleaching. Dotted circles indicate photobleached regions
1126 used for analysis. **B.** Recovery plots of fluorescence intensity and fitted curves (single
1127 exponential fit) after photobleaching for N2-N (green), N2-C (magenta) and DLL4 (blue)
1128 freely dispersed in the membrane. **C.** Diffusion coefficients derived from fluorescence
1129 recovery after photobleaching for N2-N (green), N2-C (magenta) and DLL4 (blue) freely
1130 dispersed in the membrane. **D, F, H.** Fluorescence recovery after photobleaching (FRAP)
1131 experiment, showing representative images of N2-N (**D**), N2-C (**F**), and DLL4 (**H**)
1132 engaged in synapses before and as a function of time after photobleaching. Images also
1133 show unbleached fluorophores (DLL4 in **D**, N2-N in **F**, and N2-N in **H**) as a positional
1134 reference for the synapses. Areas used for analysis of recovery are represented by dotted
1135 lines. **E, G, I.** Recovery plots of fluorescence intensity after photobleaching for N2-N (**E**),
1136 N2-C (**G**), and DLL4 (**I**) when engaged in synapses. Fluorescence intensity of unbleached
1137 components of the synapse (DLL4 in **E**, N2-N in **G**, and N2-N in **I**) were also monitored
1138 and analyzed as reference. Data are represented as mean ± standard deviation;
1139 statistical analysis in **C** was performed using Kruskal-Wallis ANOVA; ns = not significant;
1140 n = number of regions/synapses analyzed as indicated.
1141
1142 **Figure 3. Transendocytosis of NOTCH2 into DLL4 cells takes place after synapse**
1143 **formation. A.** Schematic illustrating different compositions of NOTCH2-DLL4 complexes
1144 within DLL4 cell vesicles after cell pairing. Vesicles containing N2-N:DLL4 complexes
1145 (green arrowhead) and full-length NOTCH2:DLL4 complexes (containing both N2-N and
1146 N2-C; green/magenta arrowhead) are shown. **B.** Lattice light-sheet images of a DLL4

1147 sender cell paired with a NOTCH2 receiver cell 20 minutes after contact. N2-N in green,
1148 N2-C in magenta, and DLL4 in cyan. Green arrowhead: vesicle containing only DLL4 and
1149 N2-N fluorescence. Green/magenta arrowhead: vesicle containing DLL4, N2-N, and N2-
1150 C fluorescence. **C.** Stoichiometric ratio of N2-N to DLL4 in vesicles (left), and of N2-N/N2-
1151 C in vesicles (center and right). The stoichiometric ratio for N2-N/N2-C in vesicles where
1152 N2-C was not detectable was arbitrarily set to >>20. Dotted line indicates the ratio of one
1153 observed in membrane and synapses (see Figure 1). Number of vesicles analyzed = n.
1154 Error bars represent mean ± standard deviation. **D.** Schematic (left) and real-time lattice
1155 light-sheet microscopy images from a synapse at t_0 and subsequent 1 min intervals
1156 showing movement of N2-N and DLL4 fluorescence from the synapse into the sender cell
1157 over time. Synapse at t_0 is indicated with a yellow arrowhead. N2-N is shown in green,
1158 N2-C in magenta, and DLL4 in cyan. Insets show the three channels with a 5 pixel shift
1159 of the blue channel.
1160
1161 **Figure 4. NICD nuclear entry after cell-cell contact. A.** Representative spinning disk
1162 confocal images of a NOTCH2 cell nucleus at 5 and at 60 min after contact with a DLL4
1163 cell. Images show the maximum intensity projection of five planes through the center of
1164 the nucleus. N2-N is green, the N2-C tag (inclusive of NTM, NEXT, and NICD species) is
1165 magenta, and the cell nucleus/DNA is pseudocolored blue (SiR-DNA). Nuclei are outlined
1166 with yellow lines. **B,C.** Quantitative analysis of the nuclear N2-C concentration (nM)
1167 before sender cell contact (0 min), and at 5 and 60 min after contact. Data are shown as
1168 a scatter plot in **B**, and lines are drawn to connect paired concentration measurements at
1169 5 and 60 min for each nucleus analyzed in **C**. Error bars in **B** represent mean ± standard
1170 deviation. Statistical analysis in **B** was performed using Kruskal-Wallis one-way ANOVA

1171 and in **C** using Wilcoxon matched-pairs signed rank test. ns = $p>0.05$; **** = $p<0.0001$, n
1172 = number of analyzed nuclei.
1173
1174 **Figure 5. Real time visualization of events after cell pairing. A.** Representative lattice
1175 light-sheet images from a time course observing a NOTCH2 cell before (0 min) and after
1176 contact with DLL4 cells (5-60 min). Panels highlight the formation and dissipation of
1177 synapses (top), the appearance of N2-N and N2-C positive vesicles in DLL4 cells (middle
1178 two rows) and the increase of N2-C associated signal in the nucleus of the NOTCH2 cell
1179 (bottom row). DLL4 cells are depicted by dotted lines (middle two rows) and the nucleus
1180 of the NOTCH2 cell, segmented using SiR-DNA labeling, is outlined with a yellow line
1181 (bottom row). N2-N is in green, the N2-C tag (NTM, NEXT, and/or NICD) is in magenta,
1182 and DLL4 in cyan. DNA was labeled using SiR-DNA and pseudocolored blue. Scale bars
1183 as indicated. **B.** Plots showing the estimated number of N2-N molecules in synapses
1184 (top), the number of molecules in DLL4-cell vesicles (middle) and the concentration (nM)
1185 of N2-C in nuclei of NOTCH2 cells (bottom) as a function of time after DLL4-cell contact.
1186 Graphs show mean ± standard deviation from n = 9 independent cell pairing events.
1187
1188 **Figure 6. Effects of chemical and genetic perturbations on synapse formation,**
1189 **transendocytosis and nuclear NICD entry. A-D.** Effects of knocking out MIB1 (*MIB1ko*)
1190 in sender cells. **A.** Pairing of parental (top) and *MIB1ko* (bottom) DLL4 sender cells with
1191 NOTCH2 receiver cells, imaged using a spinning disk confocal microscope. Schematics
1192 (left) show cells, synapses (white, indicated by the black arrowhead), vesicles in DLL4
1193 cells (black arrow), and nuclei (blue) of NOTCH2 cells. Images (right) show paired cells 5
1194 and 60 min after contact. N2-N is shown in green, N2-C in magenta, DLL4 in cyan, and
1195 the nucleus of the NOTCH2 cell is pseudocolored blue. Images show the maximal

1196 intensity projection of a 3D z-stack of 14.84 µm. **B.** Vesicles per DLL4 cell (MIB1 parental
1197 or *MIB1ko*) 60 min after NOTCH2 cell contact, assessed by manual counting. **C.**
1198 Representative images of nuclei from NOTCH2 cells co-cultured with parental or *MIB1ko*
1199 DLL4 sender cells, shown 5 and 60 min after direct contact. N2-C is shown in magenta.
1200 The images show the maximum intensity projection of five planes through the center of
1201 the nucleus. Yellow outlines denote nuclei as segmented using SiR-DNA labeling. **D.**
1202 Quantitative analysis of the N2-C concentration (nM) in nuclei from NOTCH2 cells co-
1203 cultured with parental or *MIB1ko* DLL4 sender cells at 5 and 60 min after direct contact.
1204 **E.** N2-N/N2-C stoichiometric ratios in DLL4-containing vesicles of sender cells co-cultured
1205 with untreated, GI254023X-treated, or GSI-treated NOTCH2 cells. **F.** Representative
1206 images of nuclei from untreated, GI254023X-treated, or GSI-treated NOTCH2 cells at 5
1207 and 60 min after direct contact with DLL4 cells. N2-C is shown in magenta. Yellow outlines
1208 denote nuclei as segmented using SiR-DNA labeling. Each image shows the maximum
1209 intensity projection of three planes through the center of the nucleus. **G.** Quantitative
1210 analysis of the N2-C concentration (nM) in nuclei of untreated, GI254023X-treated or GSI-
1211 treated NOTCH2 cells at 5 and 60 min after contact with sender cells. Error bars in **B** and
1212 **E** show mean ± standard deviation. Statistical analyses in **D** and **G** were performed using
1213 the Wilcoxon matched-pairs signed rank test, and in **E** using Kruskal-Wallis one-way
1214 ANOVA. Dotted line in **E** indicates the ratio of one observed in membrane and synapses
1215 (Figure 1). ns = $p>0.05$; ** = $p<0.001$, **** = $p<0.0001$, n = number of analyzed cells,
1216 nuclei or vesicles as indicated.
1217

1218 **Figure S1. SVG-A cells as Notch receiving cells. A.** Luciferase reporter gene assay
1219 for Notch-induced transcription (Malecki et al., 2006). Parental and *NOTCH2ko* SVG-A
1220 cells were co-transfected with a reporter plasmid containing firefly luciferase under control
1221 of the Notch-responsive TP1 promoter (Kurooka et al., 1998; Minoguchi et al., 1997) and
1222 an internal control Renilla luciferase plasmid (Promega) using Lipofectamine™ 2000
1223 (Invitrogen). 24 hours after transfection, these cells were co-cultured with U2OS parental
1224 cells or U2OS cells stably expressing DLL4-mCherry in presence of DMSO or GSI
1225 (Compound E). Cells were lysed 24 hours later, and the firefly and Renilla luciferase
1226 activity of each lysate was measured using a Dual Luciferase Assay Kit (Promega). The
1227 firefly/Renilla ratio was normalized to the signal for co-culture of SVG-A cells with parental
1228 U2OS cells. Plots show mean ± standard deviation from four independent biological
1229 replicates (n=4). **B.** RNA-seq analysis of genes induced in SVG-A cells seeded onto
1230 tissue culture plates coated with JAG1-Fc (200 μg/ml) at timepoints after removal of GSI
1231 (100 nM). Volcano plots compare RNA abundance at 2, 4, and 24 hours to a reference
1232 sample at t=0 subjected to a mock washout with media containing GSI. Red dots indicate
1233 significantly upregulated genes (adj. p value < 0.001, Fold Change > 1.5), while blue dots
1234 indicate significantly downregulated genes (adj. p value < 0.001, Fold Change < -1.5).
1235

1236 **Figure S2. Preparation of DMS53 DLL4-HaloTag knockin cells. A.** Analysis of Notch
1237 ligands on DMS53 cells by flow cytometry. Cells were stained using fluorescently
1238 conjugated anti-DLL1, anti-DLL4, anti-JAG1, and anti-JAG2 antibodies, using anti-IgG
1239 isotype staining as a reference. Representative histograms of stained cell populations are
1240 shown. **B.** Geometric mean fluorescence intensities (gMFI) of anti-DLL1, anti-DLL4, anti-
1241 JAG1, and anti-JAG2 stained cell populations analyzed by flow cytometry in **A**,
1242 normalized to anti-IgG isotype staining. **C.** Luciferase reporter gene assay. Parental or

1243 *NOTCH2ko* SVG-A cells were co-transfected with a reporter plasmid containing firefly
1244 luciferase under control of the Notch-responsive TP1 promoter (Kurooka et al., 1998;
1245 Minoguchi et al., 1997) and an internal control Renilla luciferase plasmid (Promega) using
1246 Lipofectamine™ 2000 (Invitrogen). 24 hours after transfection, these cells were co-
1247 cultured with DMS53 cells in the presence of DMSO or GSI (0.5 μM). Cells were lysed 24
1248 hours later, and the firefly and Renilla luciferase activity of each lysate was measured
1249 using a Dual Luciferase Assay Kit (Promega). The firefly/Renilla ratio was normalized to
1250 the signal for co-culture of SVG-A parental cells with DMS53 cells in the presence of
1251 DMSO. **D.** Schematic showing parental DLL4 and the engineered DLL4 fusion containing
1252 a C-terminal HaloTag. **E.** Sequence from the *DLL4* locus showing the C-terminal tagging
1253 site and sgRNA targeting sequence used for CRISPR/Cas9 mediated genome editing. **F.**
1254 *DLL4* genomic locus showing schematics of the repair template with homology arms,
1255 tagging site and linker used, as well as the targeted *DLL4* allele. **G.** Anti-DLL4 western
1256 blot. Lysed parental DMS53 cells, *DLL4-HaloTag* knockin DMS53 cells, and DMS53
1257 *DLL4*ko cells were probed with an anti-DLL4 antibody. GAPDH immunodetection was
1258 used as a loading control. **H.** Luciferase reporter gene assay. SVG-A cells were treated
1259 as in **C** before co-culturing with DMS53 parental, DMS53 *DLL4ko*, or DMS53 DLL4-
1260 HaloTag cells. Cells were lysed 24 hours later, and the firefly and Renilla luciferase
1261 activity of each lysate was measured using a Dual Luciferase Assay Kit (Promega). The
1262 firefly/Renilla ratio was normalized to the signal for co-culture of SVG-A cells with parental
1263 DMS53 cells. **I, J.** Flow cytometry analysis of DMS53 parental, DMS53 *DLL4ko*, and
1264 DMS53 DLL4-HaloTag cell lines. Cells were incubated with a fluorescently conjugated
1265 anti-DLL4 antibody or an anti-IgG isotype control. Representative histograms (**I**) and
1266 geometric mean fluorescence intensity plots, normalized to parental cells (**J**), are shown.
1267 **K.** Imaging of DMS53 parental cells and DMS53 DLL4-HaloTag knockin cells. Cells were

1268 imaged using a spinning disk confocal microscope when unlabeled or when labeled with
1269 JaneliaFluorX646 (JFX646). Scale bar as indicated. Data plotted in **B, C, H, and J** are
1270 shown as mean ± standard deviation, with n ≥ 3 independent biological replicates.
1271
1272 **Figure S3 Preparation of A673 JAG1-HaloTag knockin cells.** Analysis of Notch ligands
1273 on A673 cells by flow cytometry. Cells were stained using fluorescently conjugated anti-
1274 DLL1, anti-DLL4, anti-JAG1, and anti-JAG2 antibodies, using anti-IgG isotype staining as
1275 a control. Representative histograms of staining are shown. **B.** Geometric mean
1276 fluorescence intensities (gMFI) of anti-DLL1, anti-DLL4, anti-JAG1, and anti-JAG2
1277 stained cell populations analyzed by flow cytometry in **A**, normalized to anti-IgG isotype
1278 staining. **C.** Luciferase reporter gene assay. Parental or *NOTCH2ko* SVG-A cells were
1279 co-transfected with a reporter plasmid containing firefly luciferase under control of the
1280 Notch-responsive TP1 promoter (Kurooka et al., 1998; Minoguchi et al., 1997) and an
1281 internal control Renilla luciferase plasmid (Promega) using Lipofectamine™ 2000
1282 (Invitrogen). 24 hours after transfection, these cells were co-cultured with A673 cells in
1283 the presence of DMSO or GSI (0.5 μM). Cells were lysed 24 hours later, and the firefly
1284 and Renilla luciferase activity of each lysate was measured using a Dual Luciferase Assay
1285 Kit (Promega). The firefly/Renilla ratio was normalized to the signal for co-culture of SVG-
1286 A parental cells with A673 cells in the presence of DMSO. **D.** Schematic showing parental
1287 JAG1 and the engineered JAG1 fusion containing a C-terminal HaloTag. **E.** Sequence
1288 from the *JAG1* locus showing the C-terminal tagging site and sgRNA targeting sequence
1289 used for CRISPR/Cas9 mediated genome editing. **F.** *JAG1* genomic locus showing
1290 schematics of the repair template with homology arms, tagging site and linker used, as
1291 well as the targeted *JAG1* allele. **G.** Anti-JAG1 western blot. Lysed parental A673 cells,
1292 JAG1-HaloTag knockin A673 cells, and A673 *JAG1ko* cells were probed with an anti-

1293 JAG1 antibody. GAPDH immunodetection was used as a loading control. **H.** Luciferase
1294 reporter gene assay. SVG-A cells were treated as in **C** before co-culturing with A673
1295 parental, A673 *JAG1ko*, or A673 JAG1-HaloTag cells. Cells were lysed 24 hours later,
1296 and the firefly and Renilla luciferase activity of each lysate was measured using a Dual
1297 Luciferase Assay Kit (Promega). The firefly/Renilla ratio was normalized to the signal for
1298 co-culture of SVG-A cells with parental JAG1 cells. **I, J.** Flow cytometry analysis of A673
1299 parental, A673 *JAG1ko*, and A673 JAG1-HaloTag cell lines. Cells were incubated with a
1300 fluorescently conjugated anti-JAG1 antibody or an anti-IgG isotype control.
1301 Representative histograms (**I**) and geometric mean fluorescence intensity plots,
1302 normalized to parental cells (**J**), are shown. **K.** Imaging of A673 parental cells and A673
1303 JAG1-HaloTag knockin cells. Cells were imaged using a spinning disk confocal
1304 microscope when unlabeled or when labeled with JaneliaFluorX646 (JFX646). Scale bar
1305 as indicated. Data plotted in **B, C, H, and J** are shown as mean ± standard deviation, with
1306 n ≥ 3 independent biological replicates. **L.** Representative images of a synapse formed
1307 by pairing an mNeon-NOTCH2-HaloTag (labeled with JFX549) SVG-A knockin cell with
1308 a JAG1-HaloTag (labeled with JFX646) knockin A673 cell. N2-N is represented in green,
1309 N2-C in magenta, and JAG1 in cyan. Scale bars as indicated. **M.** Ratios of fluorescence
1310 intensities of signals associated with N2-N and N2-C in the membrane and of N2-N and
1311 N2-C or N2-N and JAG1 in synapses, respectively. Data plotted are shown as mean ±
1312 standard deviation. The number of synapses (n) and the number of cells analyzed are
1313 indicated. Statistical analysis was performed using Kruskal-Wallis one-way ANOVA; ns =
1314 $p>0.05$. **N.** Efficiency of synapse formation. SVG-A mNeon-NOTCH2-HaloTag cells were
1315 paired with DMS53 (DLL4) or different engineered forms of A673 (JAG1) cells.
1316

1317 **Figure S4. Tagging and screening of SVG-A NOTCH2 knockin cells. A.** NOTCH2
1318 domain organization and tagging sites. Untagged NOTCH2 (top), NOTCH2 N-terminally
1319 tagged with mNeonGreen (mNeon-NOTCH2) (middle), and NOTCH2 tagged with
1320 mNeonGreen at the N-terminus and a HaloTag at the C-terminus (mNeon-NOTCH2-
1321 HaloTag) (bottom) are shown. **B-D.** CRISPR/Cas9 genome editing at the N- and C-termini
1322 of NOTCH2. **B.** N-terminal tagging site and sgRNA targeting sequence. **C.** C-terminal
1323 tagging site and sgRNA targeting sequence. **D.** Schematic of *NOTCH2* locus, the repair
1324 templates with homology arms, tags, and linkers used, as well as the *NOTCH2* targeted
1325 allele. **E.** Western Blot of SVG-A cells with *NOTCH2* knockout (*NOTCH2ko*), parental
1326 cells, cell clone with N-terminal knockin of mNeonGreen (mNeon-NOTCH2), and the
1327 doubly tagged cell clone expressing NOTCH2 with an N-terminal mNeonGreen tag and
1328 a C-terminal HaloTag (mNeon-NOTCH2-HaloTag). The antibody recognizing the
1329 intracellular domain of NOTCH2 was used to detect the C-terminal NTM fragments of the
1330 heterodimeric receptors (middle). Detection of pre-processed proteins with the same
1331 antibody (top, longer exposure) confirms the integration of both tags. GAPDH
1332 immunodetection (bottom) was used as a loading control. **F, G.** Flow cytometry analysis
1333 of parental, *NOTCH2ko* and tagged clones. In **F**, cells were stained with an anti-NOTCH2-
1334 APC antibody (black) or unlabeled (gray), and in **G**, the mNeonGreen signal was detected
1335 in the FITC channel. **H.** Luciferase reporter gene assay. Parental, *NOTCH2ko*, and
1336 NOTCH2 knockin SVG-A cells (as indicated) were co-transfected with a reporter plasmid
1337 containing firefly luciferase under control of the Notch-responsive TP1 promoter (Kurooka
1338 et al., 1998; Minoguchi et al., 1997) and an internal control Renilla luciferase plasmid
1339 (Promega) using Lipofectamine™ 2000 (Invitrogen). 24 hours after transfection, these
1340 cells were co-cultured with U2OS cells stably expressing DLL4-mCherry. Cells were lysed
1341 24 hours later, and the firefly and Renilla luciferase activity of each lysate was measured

1342 using a Dual Luciferase Assay Kit (Promega). The firefly/Renilla ratio was normalized to
1343 the signal for co-culture of SVG-A parental cells with U2OS DLL4-mCherry cells. **I.**
1344 Fluorescence of mNeonGreen-NOTCH2 cells (right) compared to parental cell
1345 autofluorescence (left), imaged on a spinning disk confocal microscope. Scale bar as
1346 indicated. Plots in **F-H** show mean ± standard deviation from at least three independent
1347 biological replicates (n≥3).
1348
1349 **Figure S5. Microfluidics configuration for cell pairing. A.** Scheme of the photomask
1350 as used to create the PDMS chips for microfluidic cell delivery. **B.** Schematic of the
1351 microfluidics system used to initiate pairing of DLL4 (DMS53) cells with NOTCH2 (SVG-
1352 A) cells. NOTCH2 cells were seeded on a coverslip containing a PDMS chip that is
1353 connected to a cell reservoir, and labeled with a JFX dye. DLL4 cells were labeled
1354 separately with a different JFX dye, detached from a culture dish, and stored in the cell
1355 reservoir until used for pairing. Using a pressure-based controller, the DLL4 cells were
1356 delivered to the pre-plated NOTCH2 cells. A flow meter was always used to monitor the
1357 flow rate. Images of the pressure controller, tube cap, and flow meter were adapted from
1358 the Fluigent Image package (Fluigent Microfluidics™, Le Kremlin-Bicêtre, France). **B.**
1359 Positioning of the coverslip and PDMS chip when used for lattice light-sheet microscopy.
1360
1361 **Figure S6. Fluorescence of unlabeled and dye-coupled SVG-A mNeon-NOTCH2-**
1362 **HaloTag cells. A, B.** Representative images of SVG-A mNeon-NOTCH2-HaloTag cells
1363 (**A**) or parental SVG-A cells (**B**) when unlabeled, incubated with JFX549 or incubated with
1364 JFX646, acquired using 488, 561, and 640 lasers in a spinning disk confocal microscope.
1365 Images show the maximum intensity projection of z-stacks. Insets in the left upper corner
1366 are magnifications of the dashed square regions. Scale bars as indicated.

1367

1368 **Figure S7. Synapse morphology and ligand dependence. A.** Set of images
1369 representing the variability of synapses that form at sites of contact between DLL4 and
1370 NOTCH2 cells. Images show single planes of top and orthogonal views (dashed lines
1371 indicate the region used for the orthogonal views) acquired using a spinning disk confocal
1372 microscope. N2-N is in green, N2-C in magenta, and DLL4 in cyan. **B.** Luciferase reporter
1373 gene assay. Parental SVG-A cells were co-transfected with a reporter plasmid containing
1374 firefly luciferase under control of the Notch-responsive TP1 promoter (Kurooka et al.,
1375 1998; Minoguchi et al., 1997) and an internal control Renilla luciferase plasmid (Promega)
1376 using Lipofectamine™ 2000 (Invitrogen). 24 hours after transfection, these cells were co-
1377 cultured with DMS53 cells in the presence of DMSO or GSI (0.5 μM), human IgG (hIgG)
1378 antibody control, or different combinations of ligand-blocking antibodies. Cells were lysed
1379 24 hours later, and the firefly and Renilla luciferase activity of each lysate was measured
1380 using a Dual Luciferase Assay Kit (Promega). The firefly/Renilla ratio was normalized to
1381 the signal for co-culture of SVG-A parental cells with DMS53 cells in the presence of
1382 DMSO. **C.** Representative single plane spinning disk confocal images and orthogonal
1383 views (dashed lines indicate the region used for the orthogonal views) showing synapse
1384 formation between DLL4 and NOTCH2 cells when DLL1, JAG2, and JAG2 ligand-
1385 blocking antibodies are present. No synapses are formed when all ligands are blocked by
1386 antibodies. N2-N is in green, N2-C in magenta, and DLL4 in cyan. Data in **B** are plotted
1387 as mean ± standard deviation, n = 3 independent biological replicates. Synapses in **A** and
1388 **C** are indicated by yellow arrowheads; scale bars as indicated.

1389

1390 **Figure S8. NOTCH2 signaling activity is not detected in DMS53 cells. A, B.**
1391 Luciferase reporter gene assays. DLL4 (DMS53) (**A**) or NOTCH2 (SVG-A) cells (**B**) were

1392 co-transfected with a reporter plasmid containing firefly luciferase under control of the
1393 Notch-responsive TP1 promoter (Kurooka et al., 1998; Minoguchi et al., 1997) and an
1394 internal control Renilla luciferase plasmid (Promega) using Lipofectamine™ 2000
1395 (Invitrogen). In **A,** Cells were cultured alone, co-cultured with NOTCH2 cells in DMSO, or
1396 co-cultured with NOTCH2 cells in presence of GSI (0.5 μM). In **B,** Cells were cultured
1397 alone, co-cultured with DLL4 cells in DMSO, or co-cultured with DLL4 cells in presence
1398 of GSI (0.5 μM). Cells were lysed 24 hours later, and the firefly and Renilla luciferase
1399 activity of each lysate was measured using a Dual Luciferase Assay Kit (Promega). The
1400 firefly/Renilla ratio was normalized to the signal for parental cells that did not undergo co-
1401 culture (left). Data are plotted as mean ± standard deviation, n = 3 independent biological
1402 replicates.
1403
1404 **Figure S9. Calibration curves for determining the concentration of HaloTag labeled**
1405 **with JFX549 ligand. A, B.** Plots of measured fluorescence intensity as a function of
1406 HaloTag-JFX549 concentration over a concentration range of 0-20 nM. A 100 ms
1407 exposure time was used in a CCD (**A**) or sCMOS (**B**) camera. Data are plotted as mean
1408 ± standard deviation. The equations representing the best fit line to the data are shown
1409 above each plot.
1410
1411 **Figure S10. Plots of fluorescence as a function of time for nine independent cell**
1412 **pairing events. A.** Plots showing the normalized fluorescence intensity of N2-N in
1413 synapses (green), N2-N in DLL4 cell vesicles (blue) and N2-C in nuclei of NOTCH2 cells
1414 (magenta) as a function of time after DLL4 cell contact. Graphs show n = 9 independent
1415 cell pairing events as measured by lattice light-sheet microscopy. **B.** Quantitative analysis
1416 of the nuclear N2-C concentration (nM) before sender cell contact (0 min), and at 30 and

1417 60 min after contact. Lines connect data points from the same cell pairing event (n = 9,
1418 same nuclei from **A**).
1419
1420 **Figure S11. Characterization of DMS53 DLL4-HaloTag *MIB1ko* cells and influence**
1421 **of protease inhibitors on synapse formation. A.** Western blots probing for MIB1 or
1422 vinculin in DMS53 parental cells, DMS53 DLL4-HaloTag cells, and DMS53 DLL4-
1423 HaloTag *MIB1ko* cells. MIB1 knockout was achieved by excision of the first exon of *MIB1*.
1424 Immunodetection of MIB1 was performed using two different antibodies recognizing N- or
1425 C-terminal regions of MIB1. Detection of Vinculin was used as a loading control. **B.**
1426 Luciferase reporter gene assay. Parental SVG-A cells were co-transfected with a reporter
1427 plasmid containing firefly luciferase under control of the Notch-responsive TP1 promoter
1428 (Kurooka et al., 1998; Minoguchi et al., 1997) and an internal control Renilla luciferase
1429 plasmid (Promega) using Lipofectamine™ 2000 (Invitrogen). 24 hours after transfection,
1430 these cells were co-cultured with DMS53 parental cells in the presence of DMSO,
1431 GI254023X (5 μM) or GSI (0.5 μM), with DMS53 DLL4-HaloTag cells, or with DMS53
1432 DLL4-Halo;*MIB1ko* cells. Cells were lysed 24 hours later, and the firefly and Renilla
1433 luciferase activity of each lysate was measured using a Dual Luciferase Assay Kit
1434 (Promega). The firefly/Renilla ratio was normalized to the signal for co-culture of SVG-A
1435 parental cells with DMS53 cells in the presence of DMSO. Data are plotted as mean ±
1436 standard deviation, n = 3 independent biological replicates. **C**. Representative orthogonal
1437 view single plane images acquired using the spinning disk microscope of synapses
1438 between NOTCH2 and DLL4 cells when untreated, treated with GI254023X, or GSI. N2-
1439 N is green and N2-C is magenta. DLL4 and the nucleus of the NOTCH2 cell are in cyan.
1440 Yellow arrows point to the synapses in the merged and single channel images. Scale bar
1441 as indicated.

1442 **Movie legends**

1443

1444 **Movie 1. Formation of synapses at sites of cell contact.** Representative lattice light-
1445 sheet movie (orthogonal view, despeckled) showing NOTCH2 cells before (0 min) and 1
1446 to 5 min after microfluidic delivery of DLL4 cells. N2-N is colored green, N2-N is magenta,
1447 DLL4 is cyan, and DNA is pseudocolored blue. Still images of the same cell pair are
1448 shown in Figure 1D.

1449

1450 **Movie 2A. 3D reconstruction of a representative synapse (I).** A 3D reconstruction of
1451 the NOTCH2-DLL4 cell pair of Movie 1 and Figure 1D, visualized 5 min after microfluidic
1452 delivery of the DLL4 cells using a lattice light sheet microscope. N2-N is colored green,
1453 N2-C is magenta, DLL4 is cyan, and DNA is pseudocolored blue.

1454

1455 **Movie 2B. 3D reconstruction of a representative synapse (II).** A 3D reconstruction of
1456 a different NOTCH2-DLL4 cell pair, visualized 5 min after microfluidic delivery of the DLL4
1457 cells using a lattice light sheet microscope. N2-N is colored green, N2-C is magenta, DLL4
1458 is cyan.

1459

1460 **Movie 3. 3D reconstruction of a cell pair showing transendocytosis of NOTCH2 into**
1461 **DLL4 cells.** 3D reconstruction of the NOTCH2-DLL4 cell pair shown in Figure 3B,
1462 visualized 20 min after microfluidic delivery of the DLL4 cells using a lattice light sheet
1463 microscope. N2-N is colored green, N2-C is magenta, and DLL4 is cyan. Green
1464 arrowhead: vesicle containing only DLL4 and N2-N fluorescence. Green/magenta
1465 arrowhead: vesicle containing DLL4, N2-N, and N2-C fluorescence.

1466 **Movie 4. Real-time visualization of events after synapse formation.** Lattice light-sheet
1467 movie (despeckled) from a time course observing a NOTCH2 cell before (0 min) and after
1468 contact with DLL4 cells (same pairing as shown in Figure 5). N2-N is colored green, and
1469 N2-C is magenta; DLL4 and the NOTCH2 cell nucleus are cyan. First row: maximum
1470 intensity projection of a 3D z-stack of 31.20 μm of the merged image, followed by separate
1471 movies of the cyan (DLL4/NOTCH2 nucleus), green (N2-N) and magenta (N2-C)
1472 channels. Second row: (i) 3D segmentation of the synapse (silver), (ii) N2-N within DLL4
1473 cell vesicles, and (iii) the NOTCH2 cell nucleus showing the N2-C signal, followed by
1474 separate movies for (i), (ii) and (iii). Third row: Plots showing the estimated number of N2-
1475 N molecules in synapses (silver), the number of molecules in DLL4 cell vesicles (green)
1476 and the concentration (nM) of N2-C in nuclei of NOTCH2 cells (magenta) as a function of
1477 time after contact with the DLL4 cell (same graphs as Figure 5). Graphs show mean ±
1478 standard deviation from n = 9 independent cell pairing events. In the first and second
1479 rows, silver arrowheads indicate the synapse location and green arrowheads indicate N2-
1480 N transendocytosis into the DLL4 cell.
1481
1482 **Movie 5. Real-time visualization of events after synapse formation with 3D**
1483 **reconstruction.** Lattice light-sheet movie (despeckled) from a time course observing a
1484 NOTCH2 cell before (0 min) and after contact with DLL4 cells (same pairing as in Figure
1485 5 and Movie 4). N2-N is colored green, and N2-C is magenta; DLL4 and the NOTCH2
1486 cell nucleus are cyan. Top row: Maximum intensity projection of an 3D z-stack of 31.20
1487 μm (left) and 3D visualization (right) of the NOTCH2 cell (dark grey), with segmentation
1488 of (i) synapse (gold), (ii) N2-N (green) within DLL4 cell vesicles and (iii) the NOTCH2 cell
1489 nucleus showing the N2-C signal. Bottom row: Plots showing the estimated number of
1490 N2-N molecules in synapses (gold), the number of N2-N molecules in DLL4 cell vesicles

1491 (green) and the concentration (nM) of N2-C in nuclei of NOTCH2 cells (magenta) as a
1492 function of time after contact with DLL4 cells (same graphs as Figure 5, Movie 4). Graphs
1493 show mean ± standard deviation from n = 9 independent cell pairing events.

Figure 1

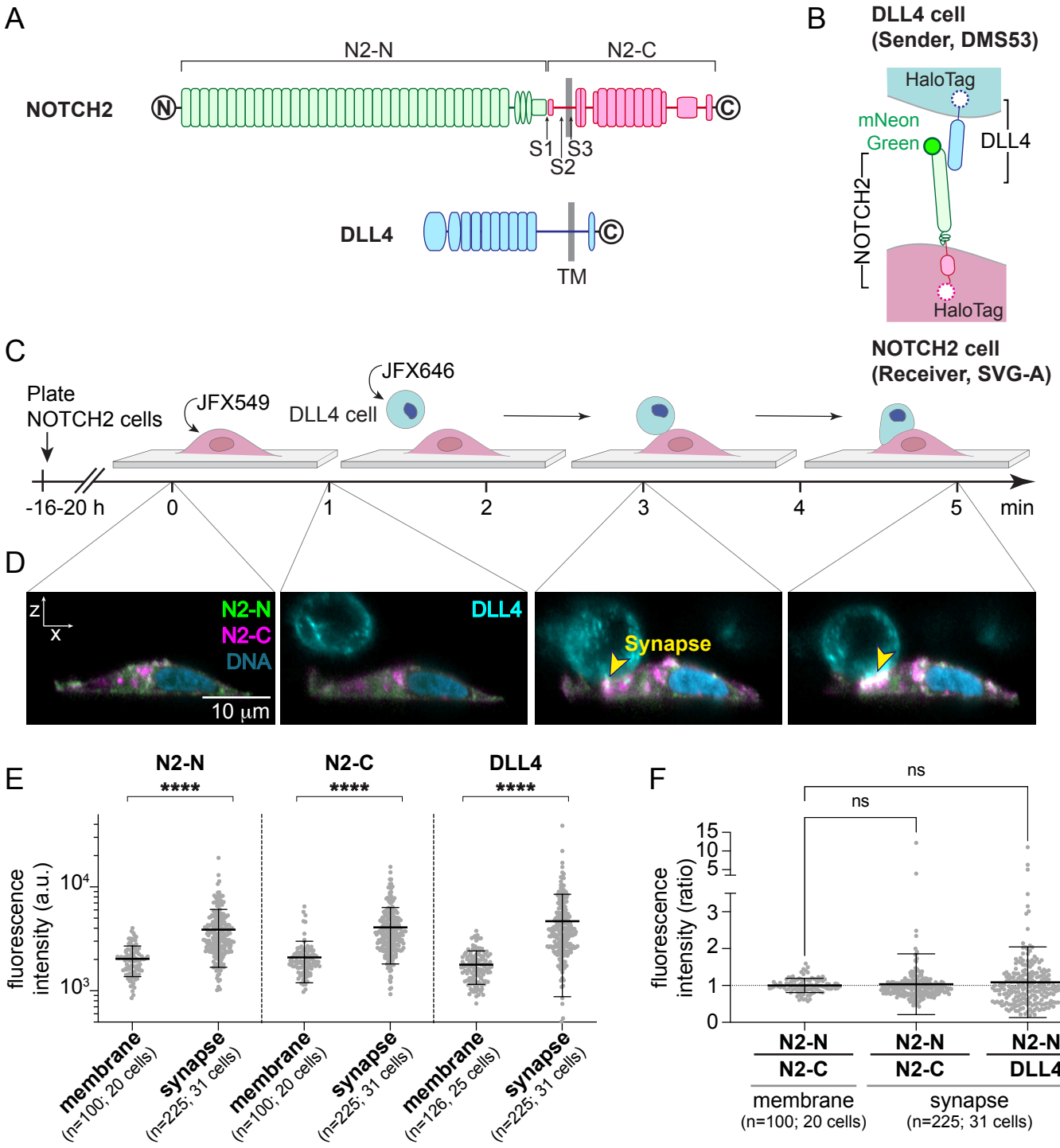
A
N2-N
N2-C
NOTCH2
N
C
S1
S2
S3
DLL4
C
TM
B
DLL4 cell
(Sender, DMS53)
HaloTag
mNeon
Green
DLL4
NOTCH2
HaloTag
NOTCH2 cell
(Receiver, SVG-A)
C
Plate
NOTCH2 cells
JFX549
DLL4 cell
JFX646
-16-20 h
0
1
2
3
4
5
min
D
z
x
N2-N
N2-C
DNA
10 µm
DLL4
Synapse
E
N2-N
N2-C
DLL4
****
****
****
fluorescence
intensity (a.u.)
10^4
10^3
membrane
(n=100; 20 cells)
synapse
(n=225; 31 cells)
membrane
(n=100; 20 cells)
synapse
(n=225; 31 cells)
membrane
(n=126, 25 cells)
synapse
(n=225; 31 cells)
F
ns
ns
fluorescence
intensity (ratio)
15
10
5
3
2
1
0
N2-N
N2-C
N2-N
N2-C
N2-N
DLL4
membrane
(n=100; 20 cells)
synapse
(n=225; 31 cells)

Figure 2

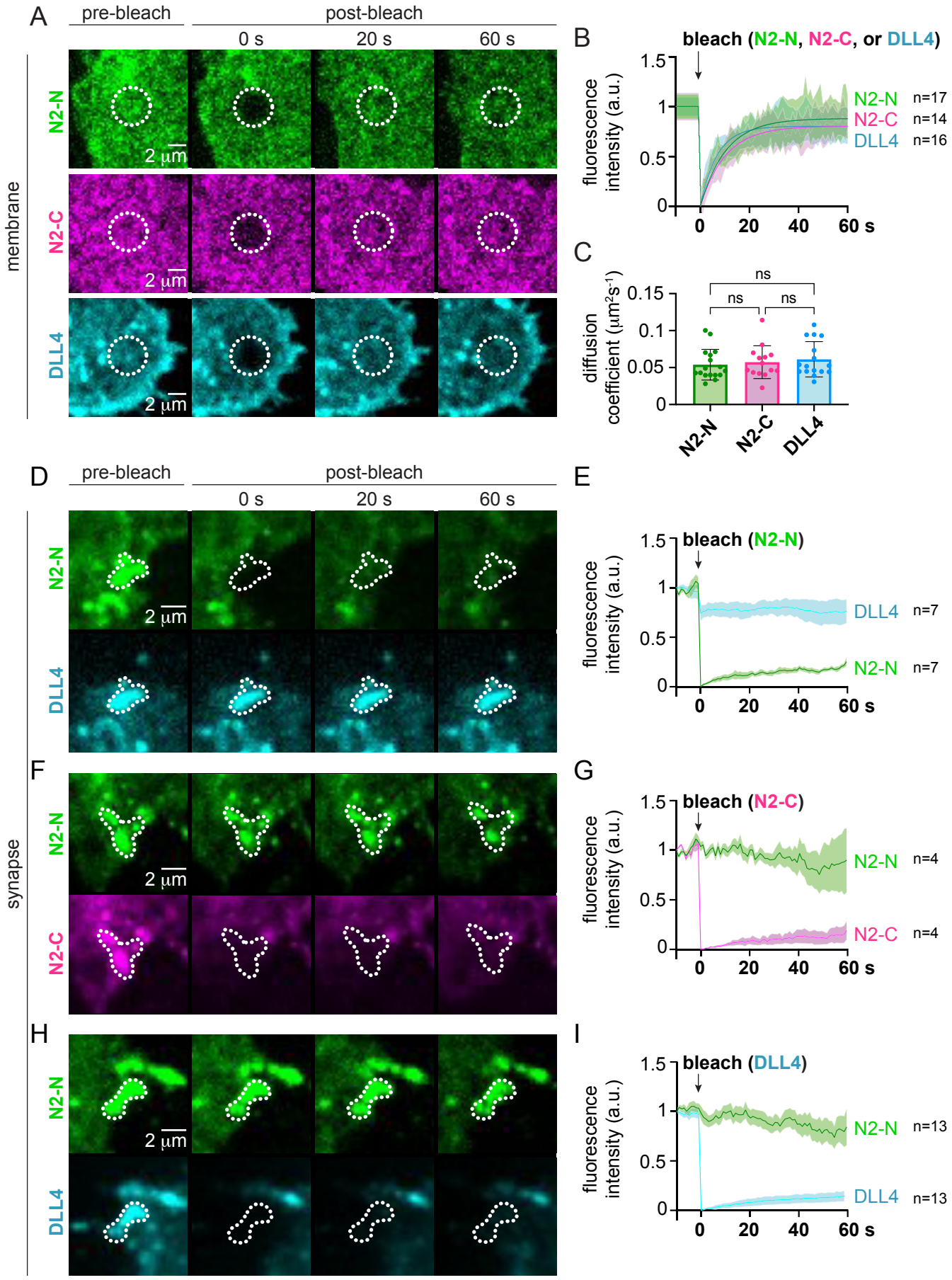
A
pre-bleach
post-bleach
0 s
20 s
60 s
membrane
N2-N
N2-C
DLL4
2 µm
B
bleach (N2-N, N2-C, or DLL4)
fluorescence intensity (a.u.)
N2-N n=17
N2-C n=14
DLL4 n=16
C
diffusion coefficient (µm²s⁻¹)
ns
N2-N
N2-C
DLL4
D
synapse
E
bleach (N2-N)
DLL4 n=7
N2-N n=7
F
G
bleach (N2-C)
N2-N n=4
N2-C n=4
H
I
bleach (DLL4)
N2-N n=13
DLL4 n=13
60 s

Figure 3

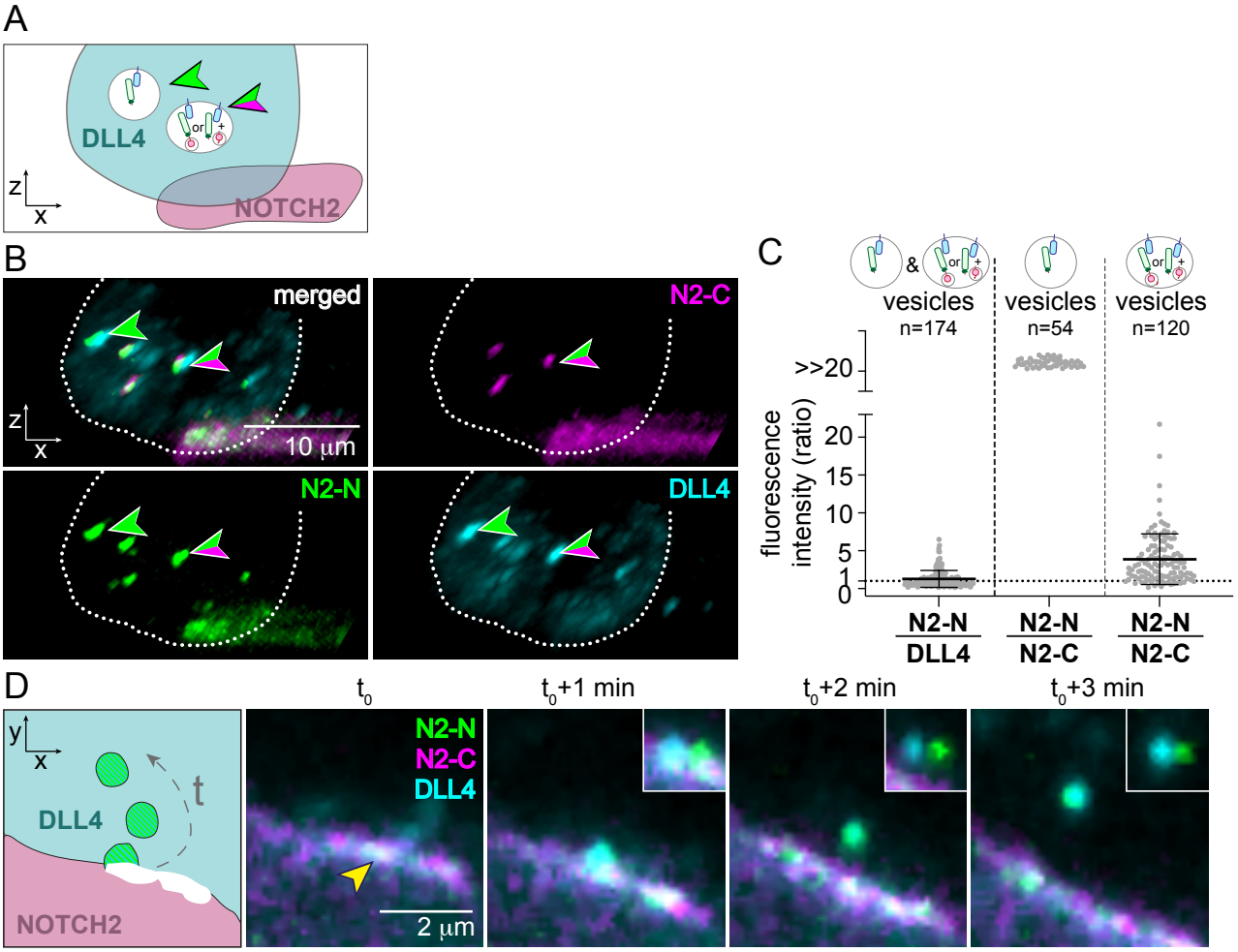
A
DLL4
NOTCH2
z
x
B
merged
N2-C
N2-N
DLL4
10 µm
C
vesicles
n=174
vesicles
n=54
vesicles
n=120
>>20
fluorescence intensity (ratio)
20
15
10
5
1
0
N2-N
DLL4
N2-N
N2-C
N2-N
N2-C
D
t0
t0+1 min
t0+2 min
t0+3 min
y
x
t
DLL4
NOTCH2
N2-N
N2-C
DLL4
2 µm

Figure 4

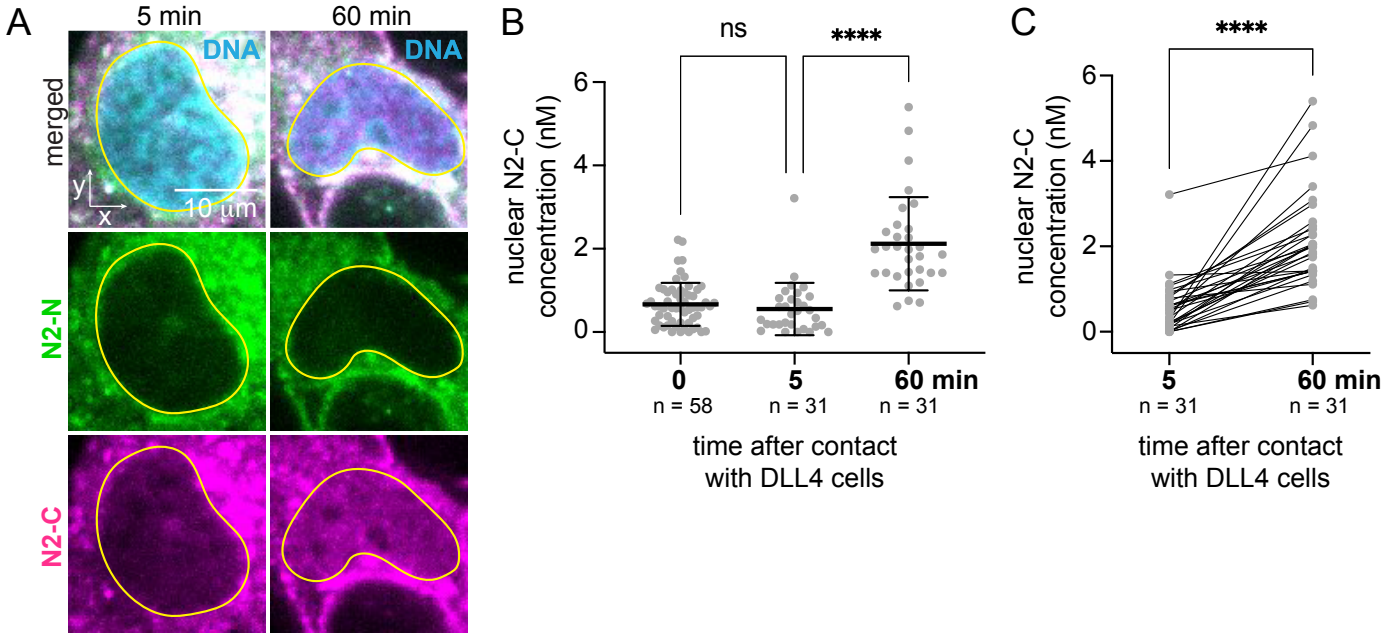
A
5 min
60 min
DNA
DNA
merged
y
x
10 µm
N2-N
N2-C
B
ns
****
nuclear N2-C concentration (nM)
6
4
2
0
0
n = 58
5
n = 31
60 min
n = 31
time after contact with DLL4 cells
C
****
nuclear N2-C concentration (nM)
6
4
2
0
5
n = 31
60 min
n = 31
time after contact with DLL4 cells

Figure 5

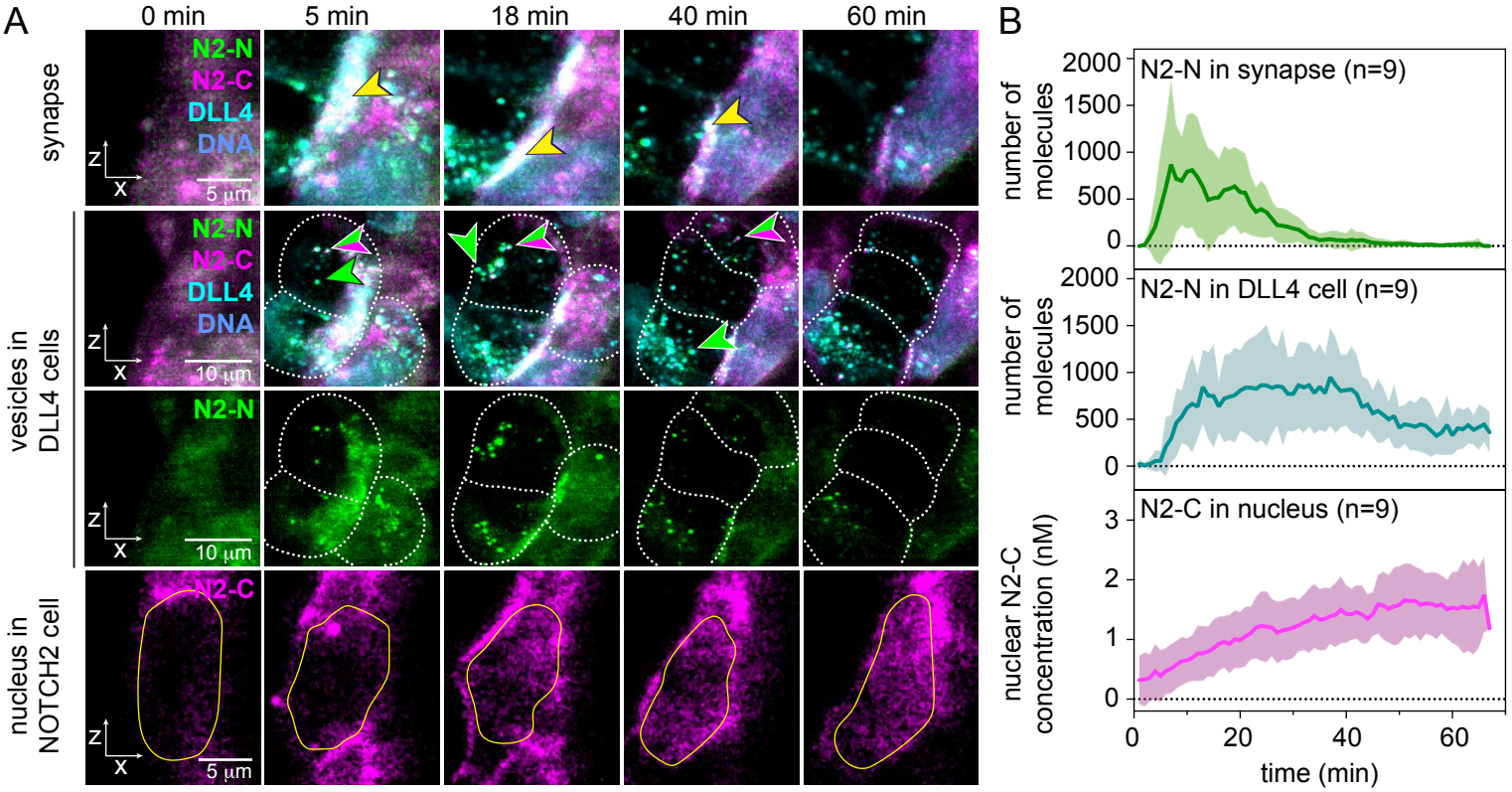
A
0 min
5 min
18 min
40 min
60 min
synapse
vesicles in DLL4 cells
nucleus in NOTCH2 cell
N2-N
N2-C
DLL4
DNA
z
x
5 µm
10 µm
B
N2-N in synapse (n=9)
N2-N in DLL4 cell (n=9)
N2-C in nucleus (n=9)
number of molecules
nuclear N2-C concentration (nM)
time (min)
0
500
1000
1500
2000
1
2
3
20
40
60

Figure 6

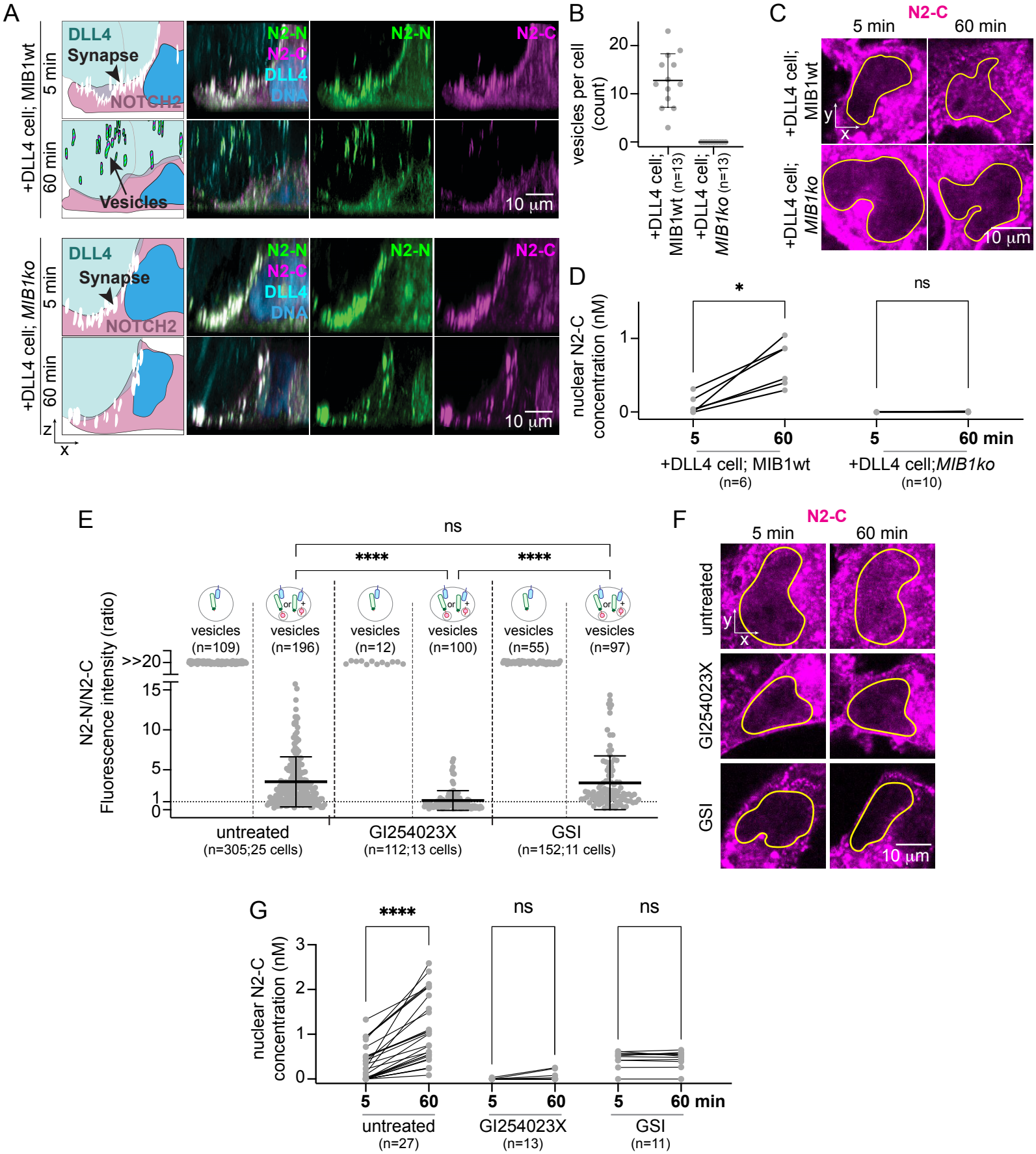
A
+DLL4 cell; MIB1wt
5 min
60 min
DLL4
Synapse
NOTCH2
Vesicles
N2-N
N2-C
DLL4
DNA
10 µm
+DLL4 cell; MIB1ko
z
x
B
vesicles per cell (count)
+DLL4 cell; MIB1wt (n=13)
+DLL4 cell; MIB1ko (n=13)
C
N2-C
5 min
60 min
+DLL4 cell; MIB1wt
+DLL4 cell; MIB1ko
y
x
10 µm
D
nuclear N2-C concentration (nM)
*
ns
5
60
60 min
+DLL4 cell; MIB1wt (n=6)
+DLL4 cell;MIB1ko (n=10)
E
ns
****
****
vesicles (n=109)
vesicles (n=196)
vesicles (n=12)
vesicles (n=100)
vesicles (n=55)
vesicles (n=97)
N2-N/N2-C Fluorescence intensity (ratio)
untreated (n=305;25 cells)
GI254023X (n=112;13 cells)
GSI (n=152;11 cells)
F
N2-C
5 min
60 min
untreated
GI254023X
GSI
10 µm
G
****
ns
ns
nuclear N2-C concentration (nM)
untreated (n=27)
GI254023X (n=13)
GSI (n=11)

Figure S1

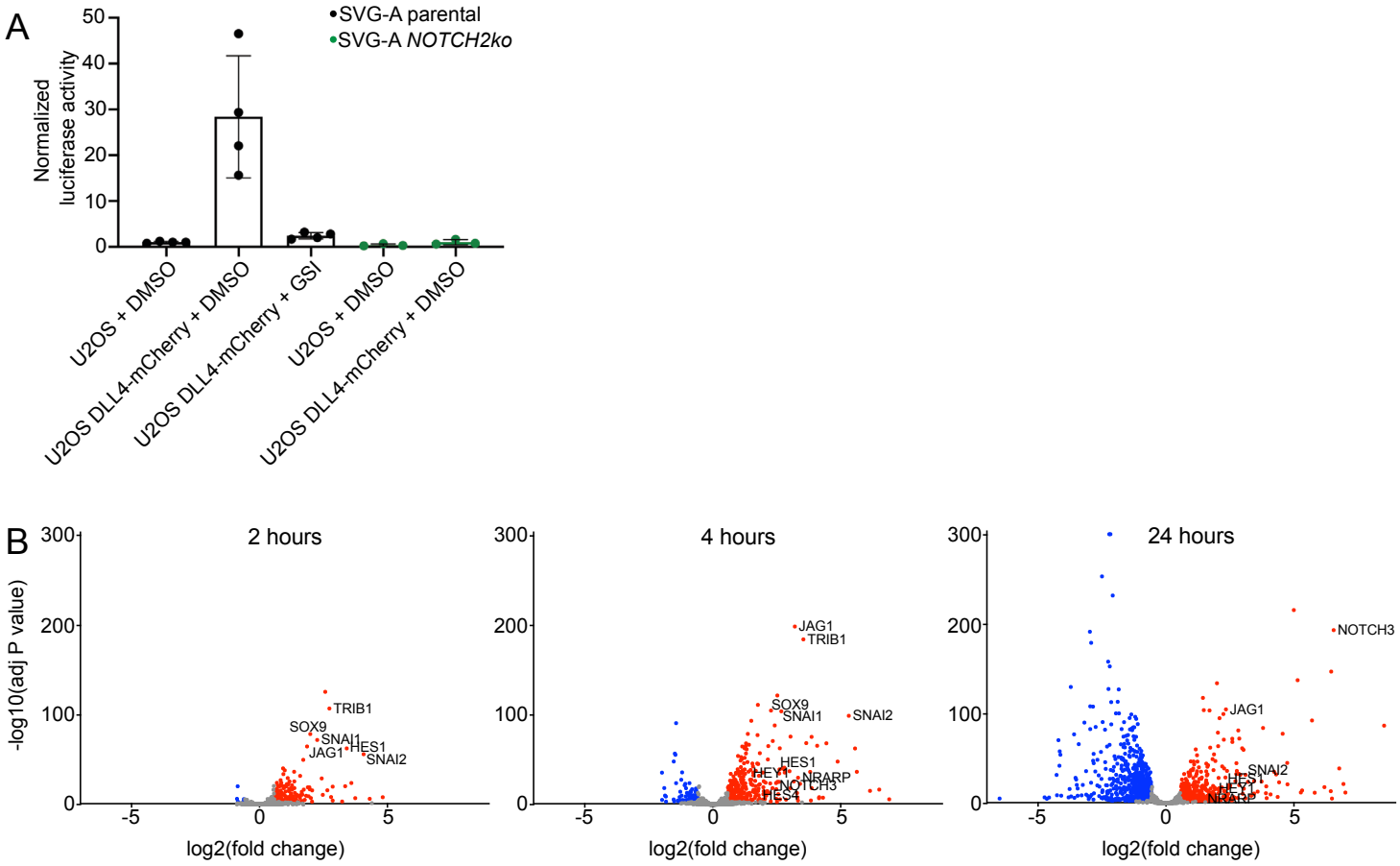
A
SVG-A parental
SVG-A NOTCH2ko
Normalized luciferase activity
50
40
30
20
10
0
U2OS + DMSO
U2OS DLL4-mCherry + DMSO
U2OS DLL4-mCherry + GSI
U2OS + DMSO
U2OS DLL4-mCherry + DMSO
B
2 hours
4 hours
24 hours
-log10(adj P value)
300
200
100
0
-5
0
5
log2(fold change)
TRIB1
SOX9
SNAI1
JAG1
HES1
SNAI2
HEY1
NRARP
NOTCH3
HES4
NOTCH3

Figure S2

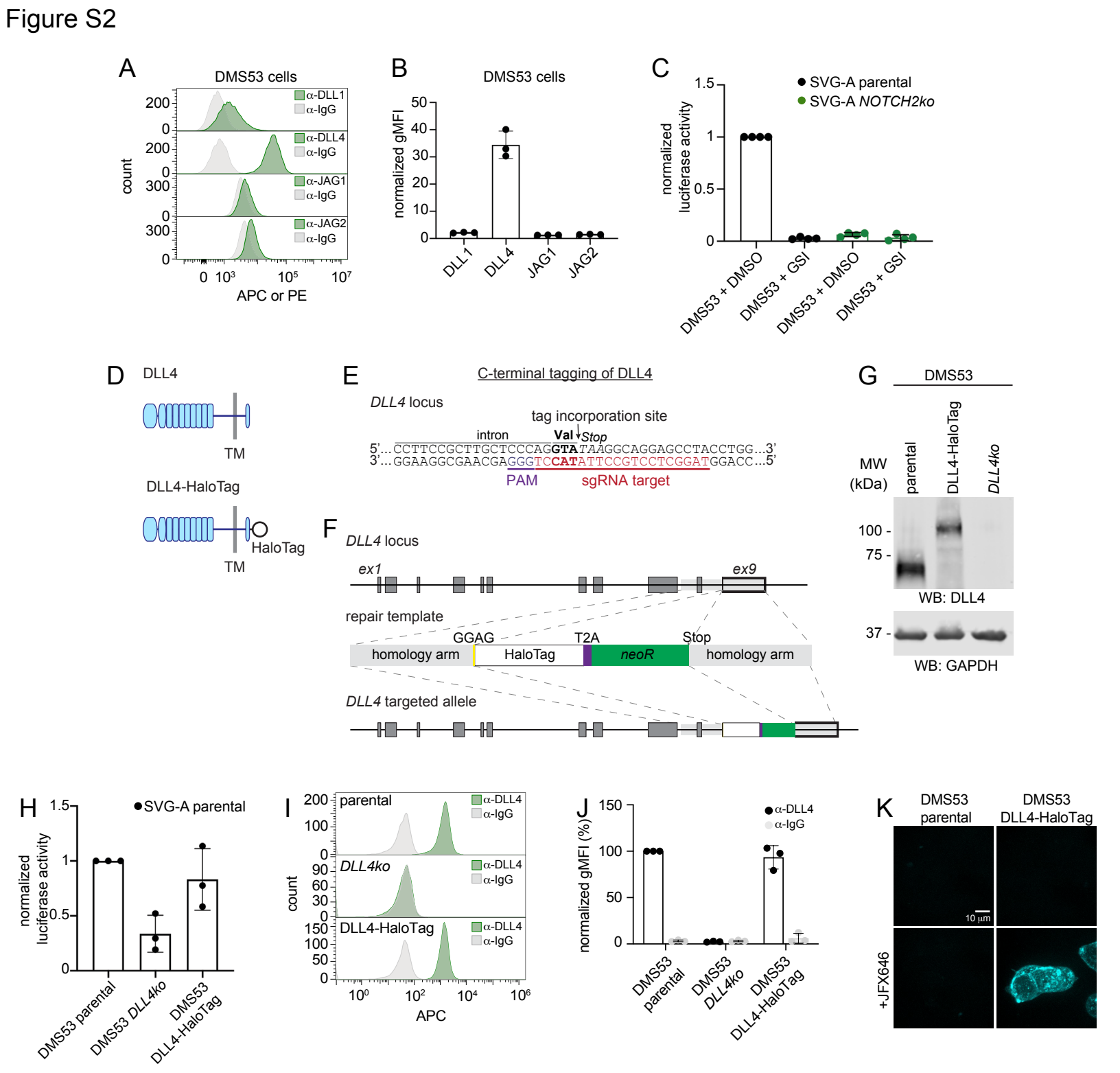
A
DMS53 cells
α-DLL1
α-IgG
α-DLL4
α-IgG
α-JAG1
α-IgG
α-JAG2
α-IgG
count
APC or PE
B
DMS53 cells
normalized gMFI
DLL1
DLL4
JAG1
JAG2
C
SVG-A parental
SVG-A NOTCH2ko
normalized luciferase activity
DMS53 + DMSO
DMS53 + GSI
DMS53 + DMSO
DMS53 + GSI
D
DLL4
TM
DLL4-HaloTag
HaloTag
TM
E
C-terminal tagging of DLL4
DLL4 locus
tag incorporation site
intron
Val
Stop
5'...CCTTCCGCTTGCTCCCAGGTATAAGGCAGGAGCCTACCTGG...3'
3'...GGAAGGCGAACGAGGGTCCATATTCCGTCCTCGGATGGACC...5'
PAM
sgRNA target
F
DLL4 locus
ex1
ex9
repair template
GGAG
T2A
Stop
homology arm
HaloTag
neoR
homology arm
DLL4 targeted allele
G
DMS53
MW (kDa)
parental
DLL4-HaloTag
DLL4ko
100 -
75 -
WB: DLL4
37 -
WB: GAPDH
H
SVG-A parental
normalized luciferase activity
DMS53 parental
DMS53 DLL4ko
DMS53 DLL4-HaloTag
I
parental
α-DLL4
α-IgG
DLL4ko
α-DLL4
α-IgG
DLL4-HaloTag
α-DLL4
α-IgG
count
APC
J
α-DLL4
α-IgG
normalized gMFI (%)
DMS53 parental
DMS53 DLL4ko
DMS53 DLL4-HaloTag
K
DMS53 parental
DMS53 DLL4-HaloTag
10 µm
+JFX646

Figure S3

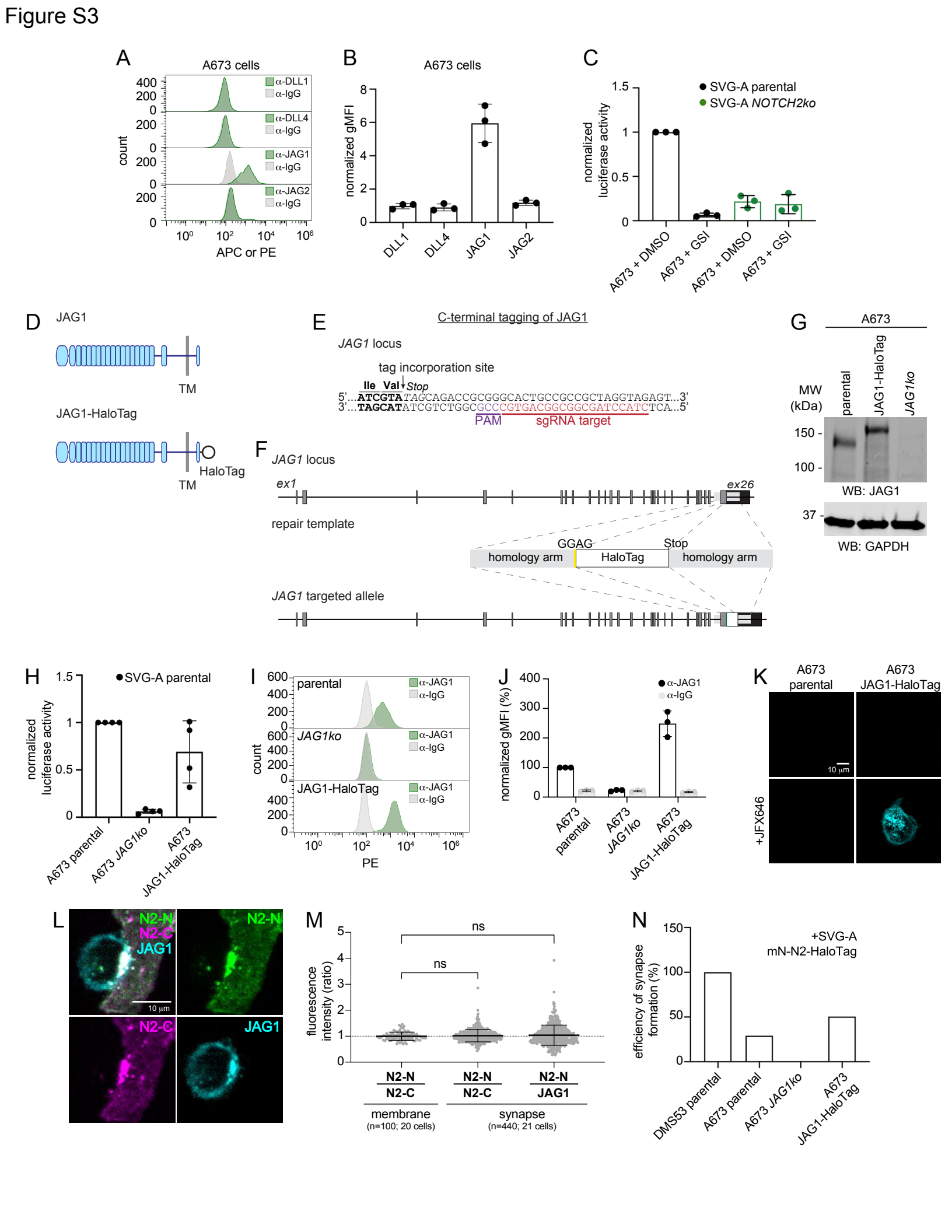
A
A673 cells
α-DLL1
α-IgG
α-DLL4
α-IgG
α-JAG1
α-IgG
α-JAG2
α-IgG
count
APC or PE
B
A673 cells
normalized gMFI
DLL1
DLL4
JAG1
JAG2
C
SVG-A parental
SVG-A NOTCH2ko
normalized luciferase activity
A673 + DMSO
A673 + GSI
A673 + DMSO
A673 + GSI
D
JAG1
TM
JAG1-HaloTag
HaloTag
TM
E
C-terminal tagging of JAG1
JAG1 locus
tag incorporation site
Ile Val Stop
5'...ATCGTATAGCAGACCGCGGGCACTGCCGCCGCTAGGTAGAGT...3'
3'...TAGCATATCGTCTGGCGCCCGTGACGGCGGCGATCCATCTCA...5'
PAM
sgRNA target
F
JAG1 locus
ex1
ex26
repair template
GGAG
Stop
homology arm
HaloTag
homology arm
JAG1 targeted allele
G
A673
parental
JAG1-HaloTag
JAG1ko
MW (kDa)
150 -
100 -
WB: JAG1
37 -
WB: GAPDH
H
SVG-A parental
normalized luciferase activity
A673 parental
A673 JAG1ko
A673 JAG1-HaloTag
I
parental
JAG1ko
JAG1-HaloTag
α-JAG1
α-IgG
count
PE
J
α-JAG1
α-IgG
normalized gMFI (%)
A673 parental
A673 JAG1ko
A673 JAG1-HaloTag
K
A673 parental
A673 JAG1-HaloTag
10 µm
+JFX646
L
N2-N
N2-C
JAG1
10 µm
N2-N
N2-C
JAG1
M
ns
ns
fluorescence intensity (ratio)
N2-N
N2-C
N2-N
N2-C
N2-N
JAG1
membrane
(n=100; 20 cells)
synapse
(n=440; 21 cells)
N
+SVG-A
mN-N2-HaloTag
efficiency of synapse formation (%)
DMS53 parental
A673 parental
A673 JAG1ko
A673 JAG1-HaloTag

Figure S4

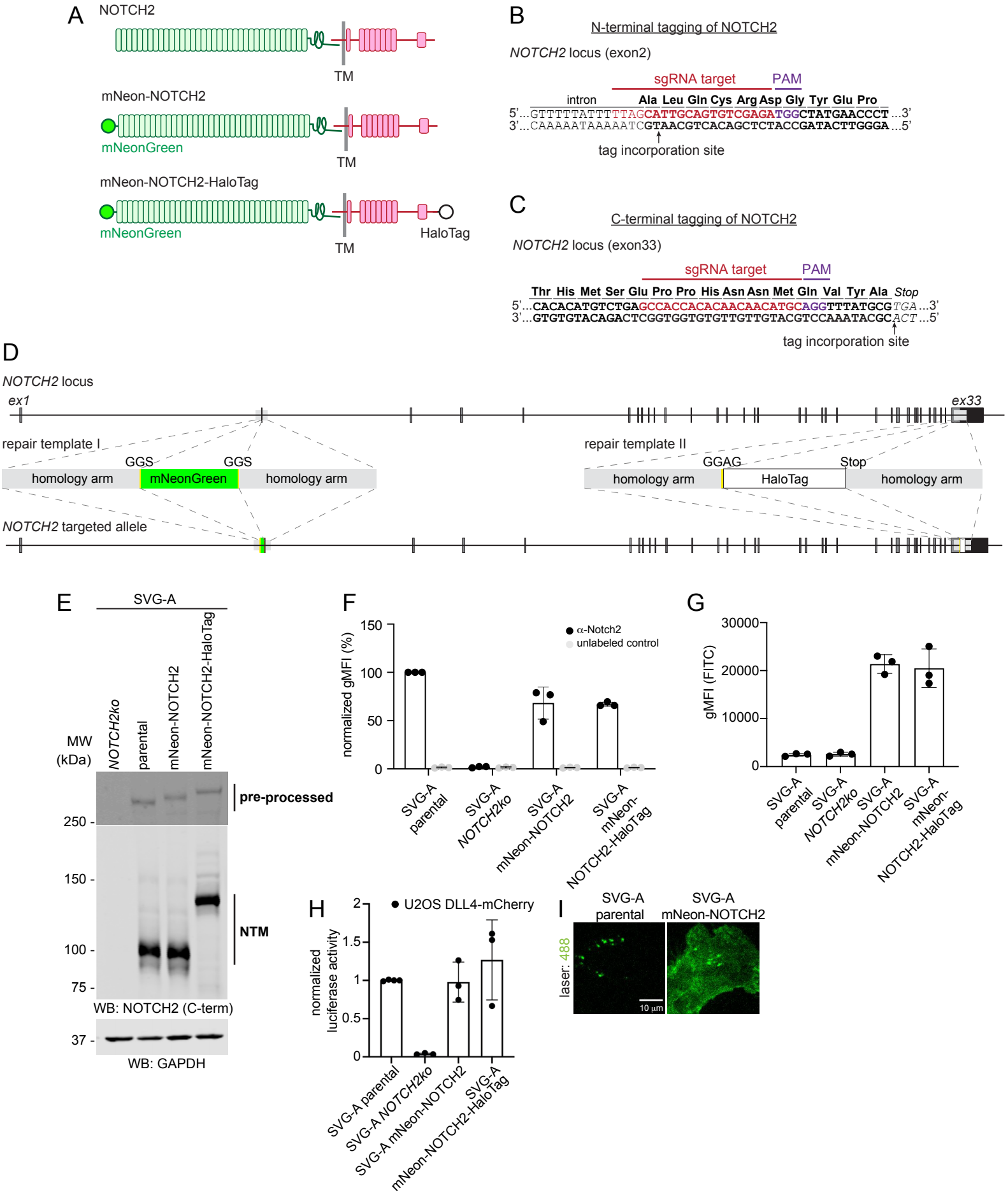
A
NOTCH2
TM
mNeon-NOTCH2
mNeonGreen
TM
mNeon-NOTCH2-HaloTag
mNeonGreen
TM
HaloTag
B
N-terminal tagging of NOTCH2
NOTCH2 locus (exon2)
sgRNA target
PAM
intron
Ala Leu Gln Cys Arg Asp Gly Tyr Glu Pro
5'...GTTTTTATTTTTAGCATTGCAGTGTCGAGATGGCTATGAACCCT...3'
3'...CAAAAATAAAAATCGTAACGTCACAGCTCTACCGATACTTGGGA...5'
tag incorporation site
C
C-terminal tagging of NOTCH2
NOTCH2 locus (exon33)
sgRNA target
PAM
Thr His Met Ser Glu Pro Pro His Asn Asn Met Gln Val Tyr Ala Stop
5'...CACACATGTCTGAGCCACCACACAACAACATGCAGGTTTATGCGTGA...3'
3'...GTGTGTACAGACTCGGTGGTGTGTTGTTGTACGTCCAAATACGCACT...5'
tag incorporation site
D
NOTCH2 locus
ex1
ex33
repair template I
GGS
GGS
homology arm
mNeonGreen
homology arm
repair template II
GGAG
Stop
homology arm
HaloTag
homology arm
NOTCH2 targeted allele
E
SVG-A
NOTCH2ko
parental
mNeon-NOTCH2
mNeon-NOTCH2-HaloTag
MW (kDa)
250
150
100
75
pre-processed
NTM
WB: NOTCH2 (C-term)
37
WB: GAPDH
F
normalized gMFI (%)
150
100
50
0
α-Notch2
unlabeled control
SVG-A parental
SVG-A NOTCH2ko
SVG-A mNeon-NOTCH2
SVG-A mNeon-NOTCH2-HaloTag
G
gMFI (FITC)
30000
20000
10000
0
SVG-A parental
SVG-A NOTCH2ko
SVG-A mNeon-NOTCH2
SVG-A mNeon-NOTCH2-HaloTag
H
U2OS DLL4-mCherry
normalized luciferase activity
2
1.5
1
0.5
0
SVG-A parental
SVG-A NOTCH2ko
SVG-A mNeon-NOTCH2
SVG-A mNeon-NOTCH2-HaloTag
I
SVG-A parental
SVG-A mNeon-NOTCH2
laser: 488
10 µm

Figure S5

A

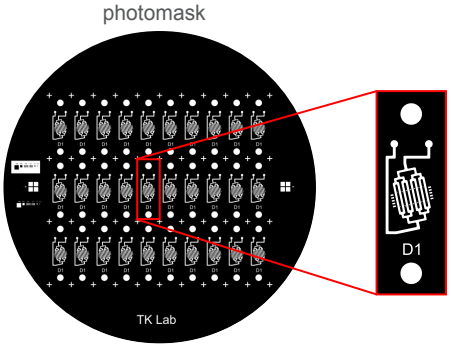

B

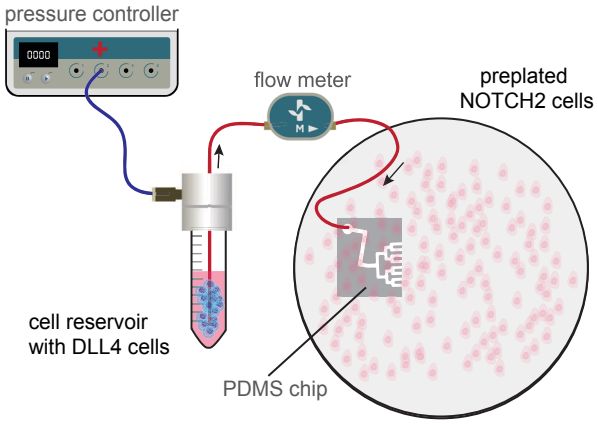

C Set-up:

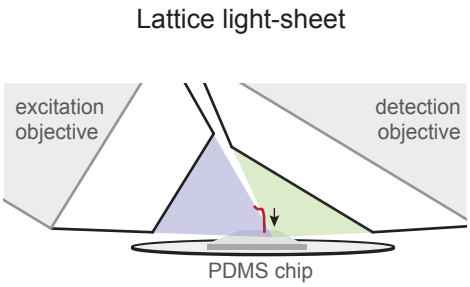

Figure S6

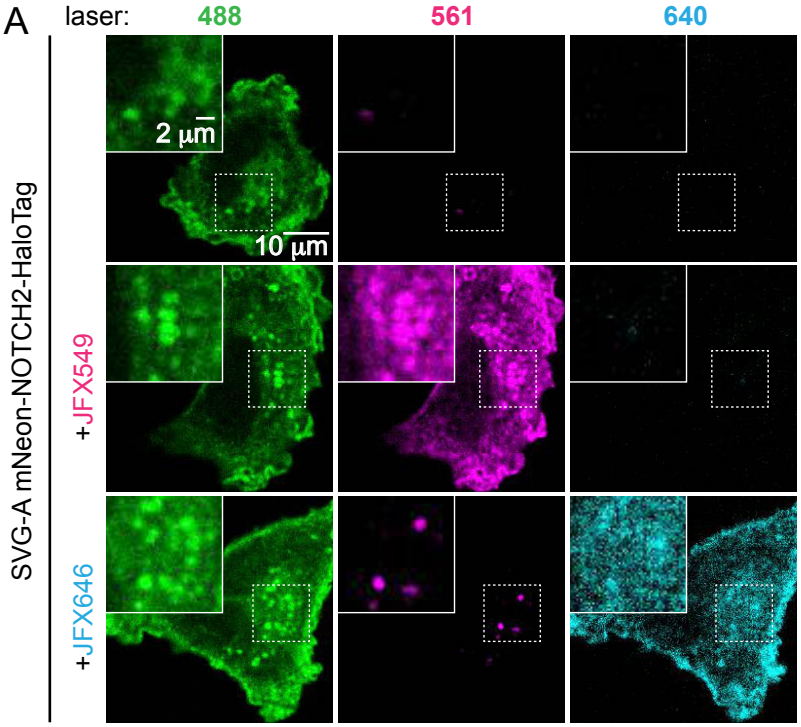
A
laser:
488
561
640
SVG-A mNeon-NOTCH2-HaloTag
+JFX549
+JFX646
2 µm
10 µm

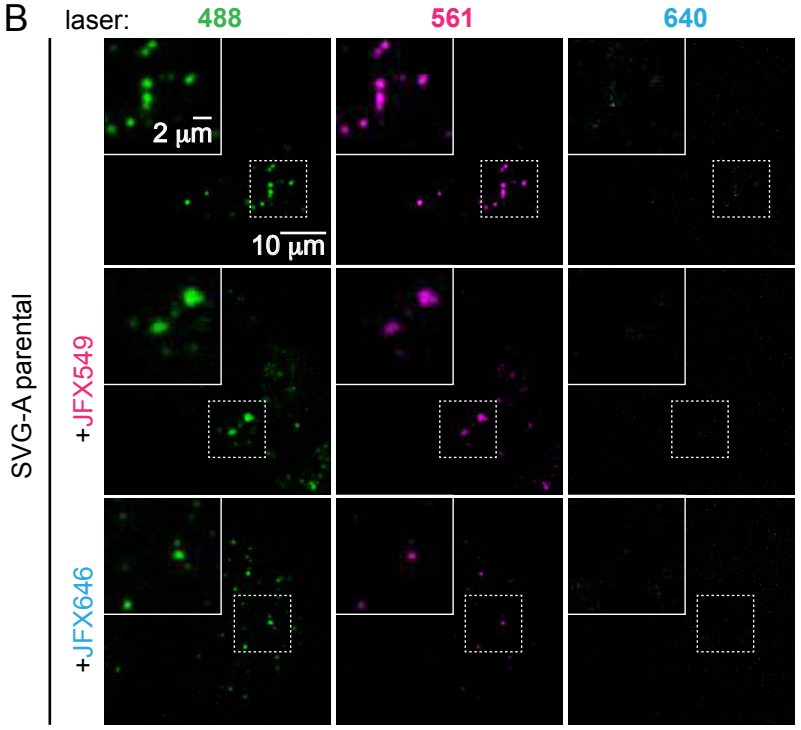
B
laser:
488
561
640
SVG-A parental
+JFX549
+JFX646
2 µm
10 µm

Figure S7

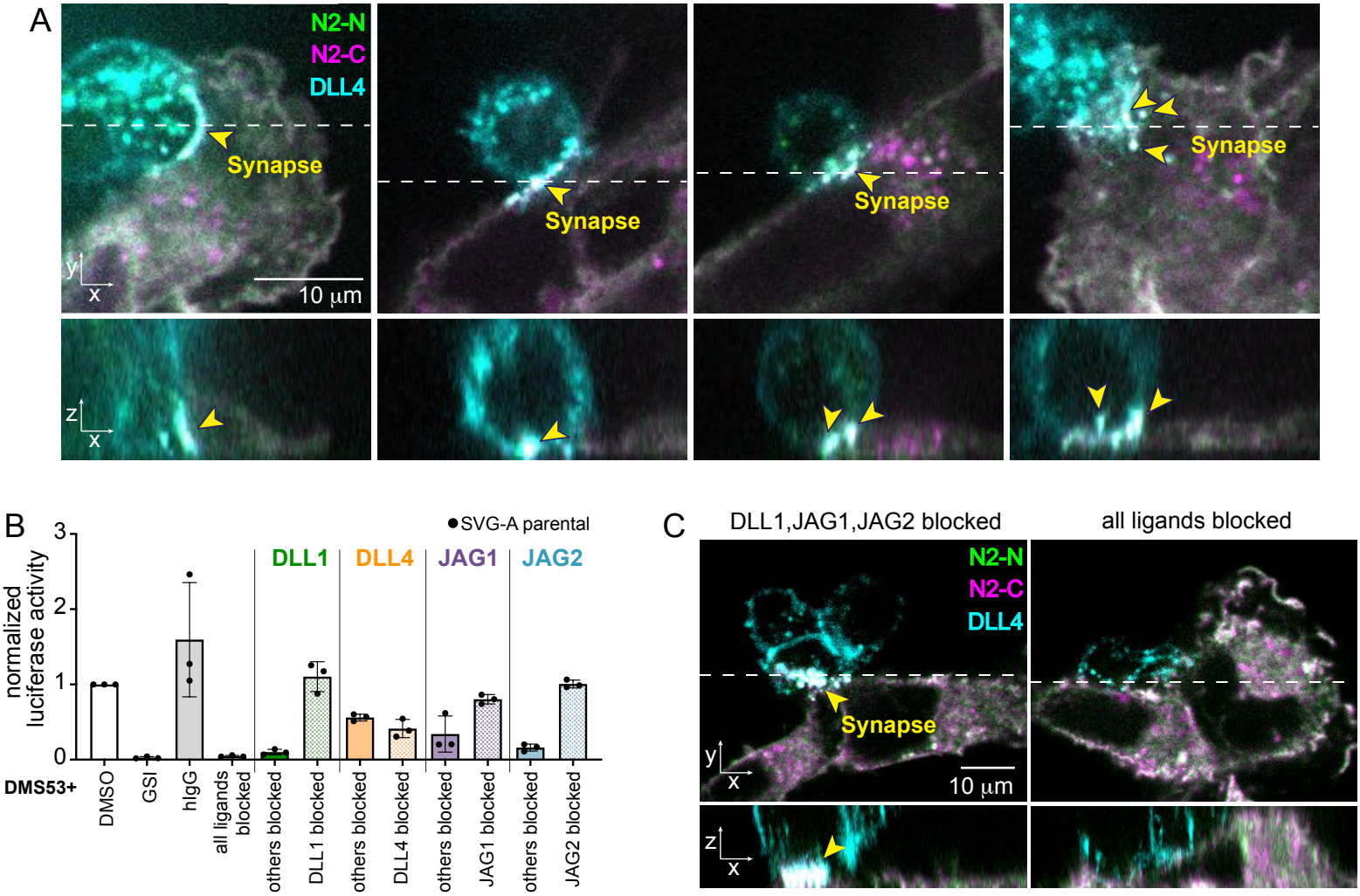
A
N2-N
N2-C
DLL4
Synapse
Synapse
Synapse
Synapse
10 μm
y
x
z
x
B
SVG-A parental
normalized luciferase activity
3
2
1
0
DLL1
DLL4
JAG1
JAG2
DMS53+
DMSO
GSI
hIgG
all ligands blocked
others blocked
DLL1 blocked
others blocked
DLL4 blocked
others blocked
JAG1 blocked
others blocked
JAG2 blocked
C
DLL1,JAG1,JAG2 blocked
all ligands blocked
N2-N
N2-C
DLL4
Synapse
10 μm
y
x
z
x

Figure S8

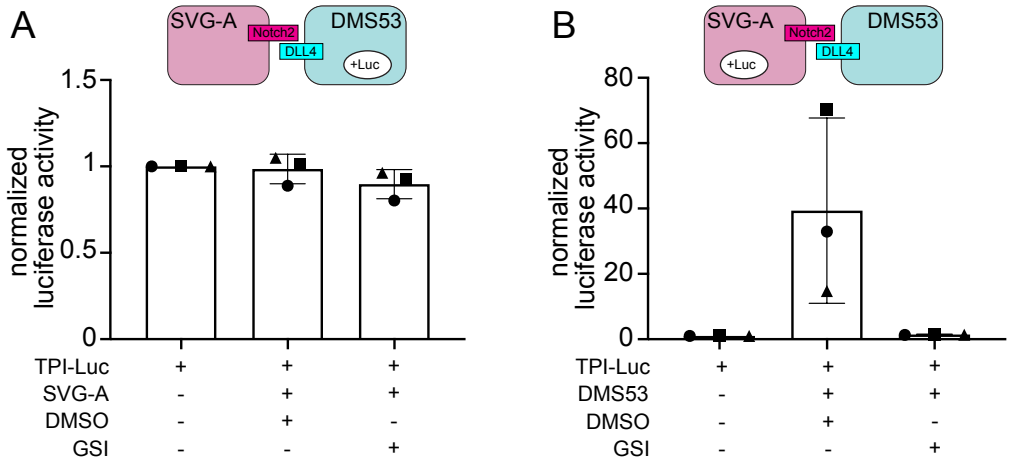
A
SVG-A
Notch2
DLL4
DMS53
+Luc
normalized luciferase activity
1.5
1
0.5
0
TPI-Luc + + +
SVG-A - + +
DMSO - + -
GSI - - +
B
SVG-A
Notch2
DLL4
DMS53
+Luc
normalized luciferase activity
80
60
40
20
0
TPI-Luc + + +
DMS53 - + +
DMSO - + -
GSI - - +

Figure S9

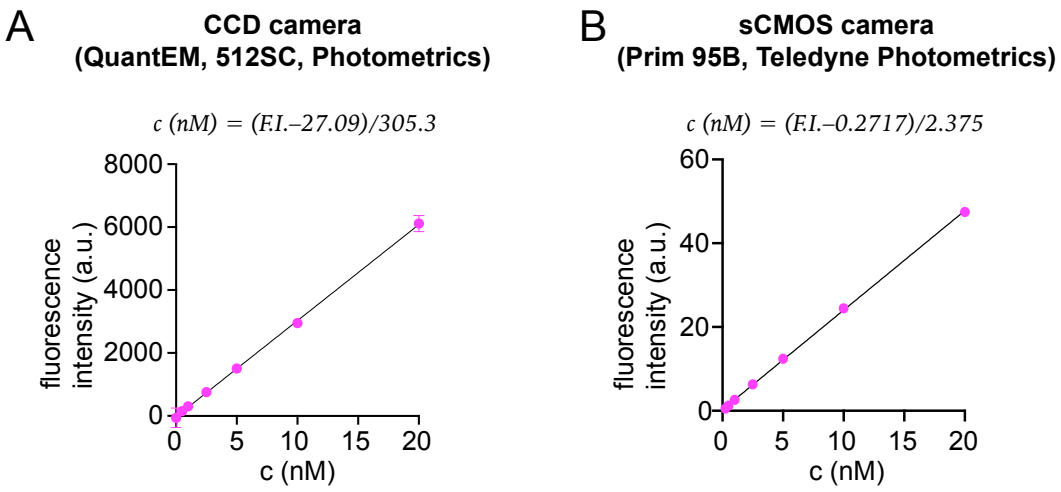
A
CCD camera
(QuantEM, 512SC, Photometrics)
c (nM) = (F.I.–27.09)/305.3
fluorescence intensity (a.u.)
8000
6000
4000
2000
0
0
5
10
15
20
c (nM)
B
sCMOS camera
(Prim 95B, Teledyne Photometrics)
c (nM) = (F.I.–0.2717)/2.375
fluorescence intensity (a.u.)
60
40
20
0
0
5
10
15
20
c (nM)

Figure S10

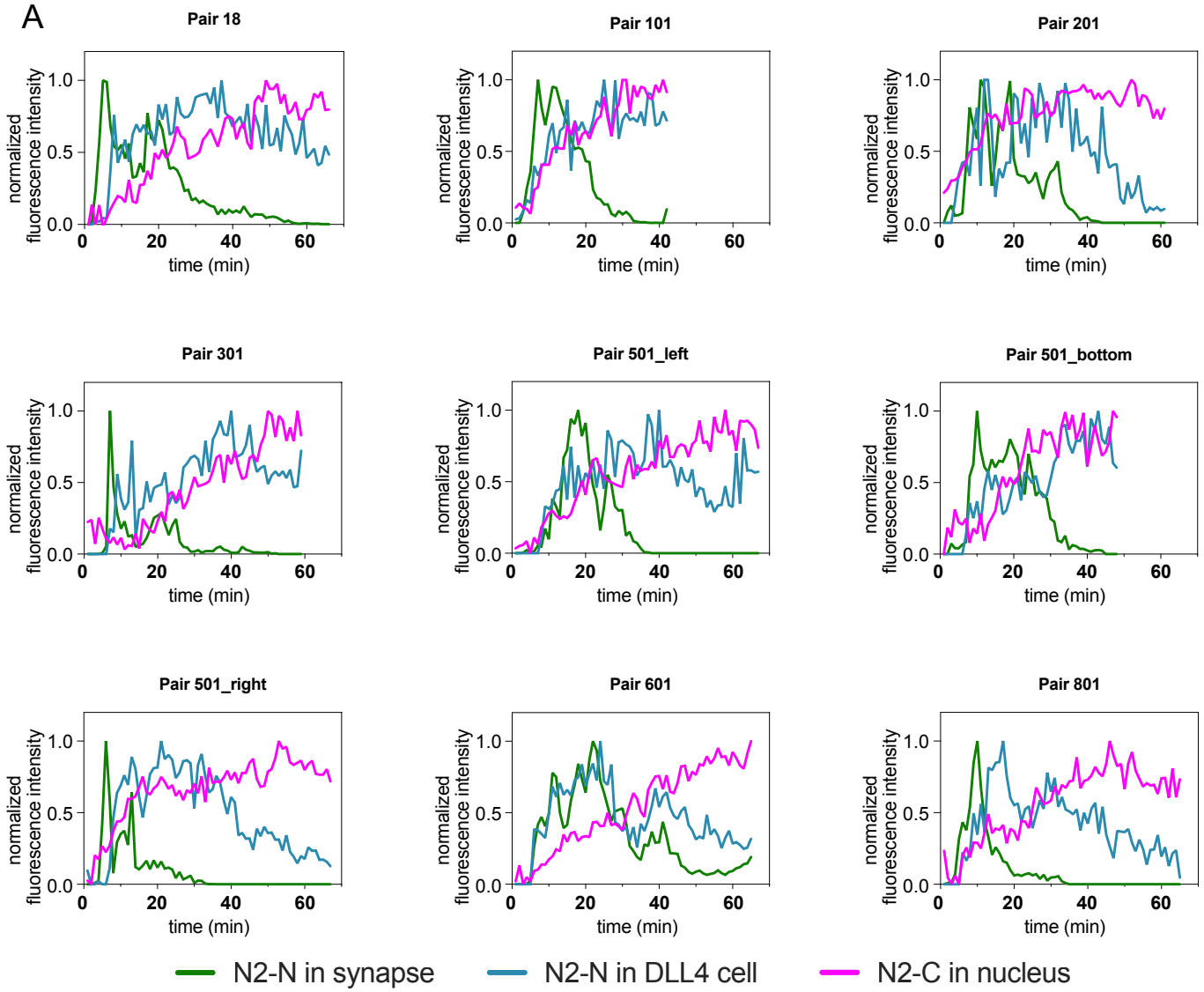
A
Pair 18
Pair 101
Pair 201
Pair 301
Pair 501_left
Pair 501_bottom
Pair 501_right
Pair 601
Pair 801
normalized fluorescence intensity
time (min)
N2-N in synapse
N2-N in DLL4 cell
N2-C in nucleus

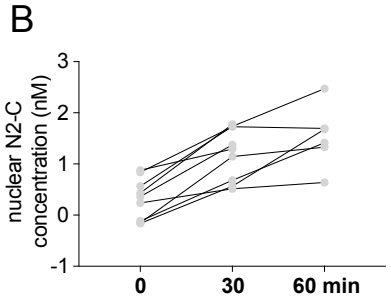
B
nuclear N2-C concentration (nM)
0
30
60 min

Figure S11

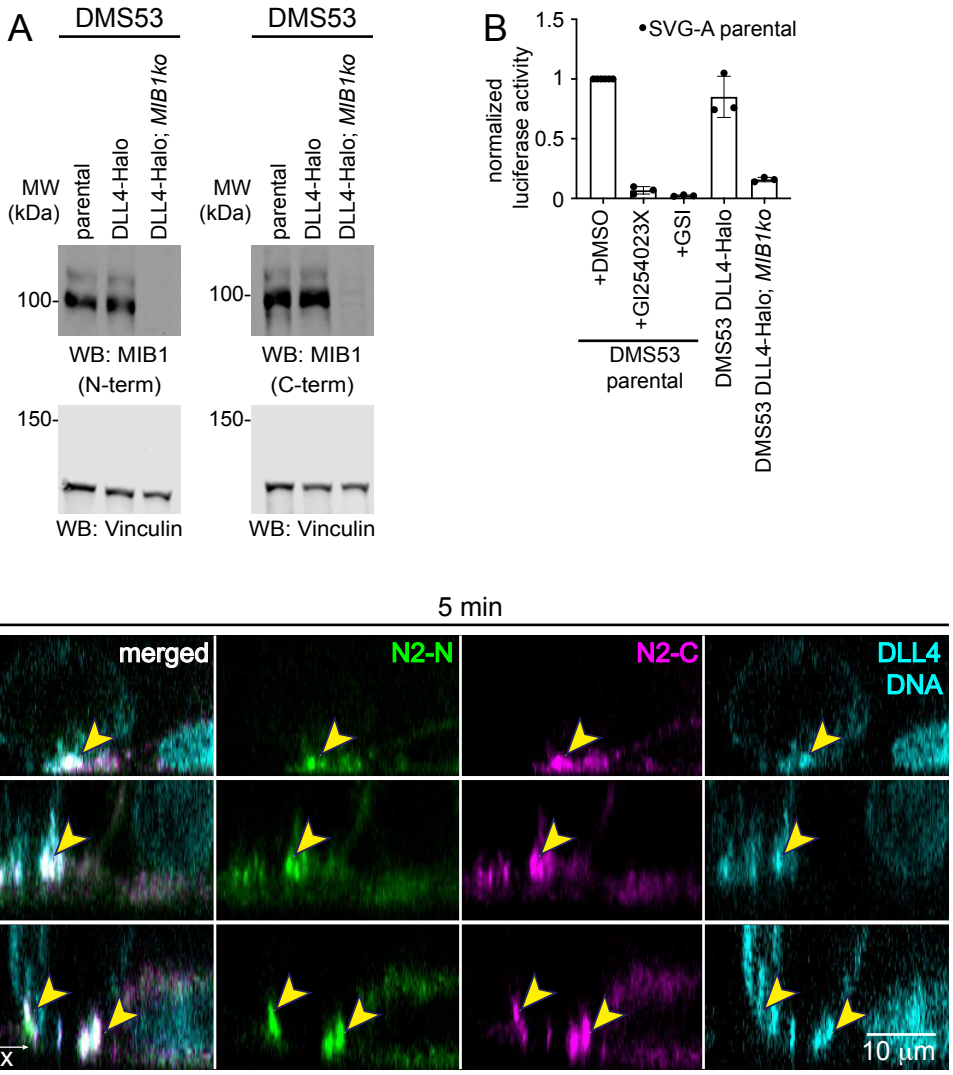
A
DMS53
DMS53
MW (kDa)
parental
DLL4-Halo
DLL4-Halo; MIB1ko
100-
WB: MIB1 (N-term)
WB: MIB1 (C-term)
150-
WB: Vinculin
B
SVG-A parental
normalized luciferase activity
1.5
1
0.5
0
+DMSO
+GI254023X
+GSI
DMS53 parental
DMS53 DLL4-Halo
DMS53 DLL4-Halo; MIB1ko
C
5 min
untreated
GI254023X
GSI
merged
N2-N
N2-C
DLL4
DNA
z
x
10 µm